Tracer dispersion in planar multipole flows

J. Koplik,[1] S. Redner,[2] and E. J. Hinch[3]

[1]*Benjamin Levich Institute and Department of Physics, City College of the City University of New York, New York, New York 10031*
[2]*Center for Polymer Studies and Department of Physics, Boston University, Boston, Massachusetts 02215*
[3]*Department of Applied Mathematics and Theoretical Physics, Cambridge University, Silver Street, Cambridge CB3 9EW, England*
(Received 13 June 1994)

We study the motion of passive Brownian tracer particles in steady two-dimensional potential flows between sources and sinks. Our primary focus is understanding the long-time properties of the transit time probability distribution for the tracer to reach the sink $p(t)$ and the influence of the flow geometry on this probability. A variety of illustrative case studies is considered. For radial potential flow in an annular region, competition between convection and diffusion leads to nonuniversal decay of the transit time probability. Dipolar and higher multipole flows are found to exhibit generic features, such as a power-law decay in $p(t)$ with an exponent determined by the multipole moment, an exponential cutoff related to stagnation points, and a "shoulder" in $p(t)$ that is related to reflection from the system boundaries. For spatially extended sinks, it is also shown that the spatial distribution of the collected tracer is independent of the overall magnitude of the flow field and that $p(t)$ decays as a power law with a geometry-dependent exponent. Our results may offer the possibility of using tracer measurements to characterize the flow geometry of porous media.

PACS number(s): 47.55.Mh, 05.40.+j

I. INTRODUCTION

A passive tracer released in flowing fluid has long been used as a diagnostic tool to monitor the characteristics of the flow field, various processes occurring within the fluid, or the material through which the fluid flows. In the case of porous media flows, particularly in groundwater or hydrocarbon recovery, tracer measurements often are the only source of internal information about the system [1–4]. For these situations, a considerable amount of experimental data, theoretical modeling, and physical insight is available, but largely in situations where the flow is one dimensional on average. In fact, in the case of porous media, the only geometrical configuration that is understood in depth is the case of flow along the axis of a long cylinder (or "core") of the material [3–6]. Typically, a tracer is introduced at one end of the sample, and convected along the core axis, and the transit time distribution is monitored upon exit at the other end. However, in many underground processes, the flow is more likely to be radial, or multipolar, than linear. Typically, fluid is pumped into an "injection" well and extracted from one or more "producing" wells. Furthermore, since geological porous media are usually highly stratified, the flow is often confined to a roughly planar permeable layer of large but finite extent. Thus the simplest plausible approximation to such an underground flow geometry is a source-sink dipole in a bounded two-dimensional region. Additional wells or fractures could modify the dipole moment or in some cases modify the multipole order of the flow field. Furthermore, although it is sometimes possible to monitor the saturation inside the sample in the laboratory [7], such measurements are rarely practicable in the field.

In this paper, we focus on the *distribution of transit times* or, equivalently, the *first-passage probability* between a source and a sink as a basic characteristic of the motion of dynamically neutral tracer in steady flows. We shall study general features of such flows, largely in two dimensions, and obtain insight into the physics underlying the transit time distribution. Our primary result is that hydrodynamic disperion in planar multipole flows differs *qualitatively* from the well-understood quasilinear case. A simple illustration of this distinction may be inferred from the general theorem [8,9] that the mean transit time for a passive tracer is given by the system volume divided by the fluid flux. In a core experiment, the volume is finite and the value of the mean time gives the average fluid velocity in the medium. However, in two or more dimensions, the volume can be effectively infinite and, correspondingly, the mean transit time can diverge. Even for finite volume systems, the flow has some radial character and the notion of a global average velocity is not necessarily meaningful. Furthermore, the shape of the transit time distribution shows a qualitative variation with the details of the system. For the pulse input of a tracer in core flows, the transit time is a Gaussian, possibly modified by details of the boundary conditions and heterogeneities in the material. As we shall see, in multipole flows, this distribution generically has a peak, followed by a geometry-dependent power-law decay which ultimately is cut off exponentially.

Mathematically, the motion of passive Brownian tracer particles is determined by their concentration $c(\mathbf{r},t)$, which satisfies the convection-diffusion equation (CDE)

$$\frac{\partial c(\mathbf{r},t)}{\partial t} + \mathbf{u}(\mathbf{r}) \cdot \nabla c(\mathbf{r},t) = D\nabla^2 c(\mathbf{r},t) , \qquad (1)$$

with the velocity field $u(r)$ independent of time and typically the diffusivity D assumed to be constant. Realistically, in porous media flows one has velocity-dependent diffusivities [4,5,10], but we shall argue in Sec. III that in neglecting this effect only some microscopic detail is lost and that our general conclusions concerning the form of the transit time distribution remain valid.

In Sec. II we consider tracer motion in radial or monopole flows in a two-dimensional annular region, where Eq. (1) can be solved in closed form. Because the radial dependence of the centrifugal term in the Laplacian and the drift term are the same, changing the strength of the flow field is tantamount to changing the spatial dimension. This gives rise to nonuniversality in the transit time properties of the system. Section III considers the prototypical "field" case of a single source and sink in a planar geometry. This section extends a previous study, by two of us (J.K. and E.J.H.) and others, which focused on a particular configuration and a corresponding experiment. Here we emphasize the shape of the transit time distribution and indicate how various features of the flow geometry manifest themselves in it. In Sec. IV we consider additional case studies, including flows of arbitrary multipolarity and flows within an absorbing wedge. Conclusions are presented in Sec. V and technical details of some derivations appear in the Appendixes.

II. FIRST PASSAGE IN RADIAL FLOWS

We begin by investigating the transit time properties of dynamically neutral tracer particles in radial potential flows $u(r) = u_0 \hat{r}/r^{d-1}$, in spherically symmetric geometries, where d is the spatial dimension. Due to the spherical symmetry, the system can be reduced to an effective one-dimensional problem in which the centrifugal term in the Laplacian acts as an inhomogeneous bias of magnitude $D(d-1)/r$. The competition between this centrifugal drift and the potential flow determines many of the interesting transit time or first-passage characteristics of the system.

This interplay is particularly delicate in two dimensions because the centrifugal and potential terms have the same dependence on r. Consequently, the form of the CDE for the two-dimensional system with u_0 finite is essentially the same as that of a system with no drift ($u_0 = 0$), but with $d \neq 2$. Due to this connection, it is relatively straightforward to derive the Laplace transform of the transit time probability for the two-dimensional system with radial drift. The crucial feature of this solution is that a change in the amplitude u_0 is equivalent to changing the spatial dimension. This leads to nonuniversal behavior for the asymptotics of transit time properties as a function of the drift.

For $d \neq 2$, the drift and centrifugal terms have different dependences on r. Consequently, there is a critical length scale $\lambda = [u_0/(d-1)D]^{1/(d-2)}$ where the two terms are of the same order. When $d > 2$, diffusion dominates over the drift for $r > \lambda$, while for $r < \lambda$ the drift dominates. These relations are reversed for $d < 2$. The transit time characteristics of a tracer particle are therefore determined by whether it is initially released in the diffusive or

convective region. While we have not been able to obtain the full time-dependent solution, we can obtain partial information which can be formulated in terms of time-independent equations. This includes, for example, the probability that a tracer particle eventually reaches an absorber as a function of the initial tracer position. The functional form of this hitting probability reflects the two above-mentioned regimes of behavior.

A. Time-dependent behavior in two dimensions

For generality, consider an annular geometry of inner and outer radii a and R, respectively, to encompass all circularly symmetric geometries. There are two generic situations to consider. In the "inner" problem, we take the inner radius as absorbing and the outer radius as reflecting. For this problem, the interesting asymptotic properties arise in the limit where $R \rightarrow \infty$. The complementary "outer" problem involves reflection at $r = a$ and absorption at $r = R$. For this situation, interesting long-time behavior arises for sufficiently strong inward drift.

Consider first the inner problem. To obtain its transit time properties, we solve the CDE in the velocity field

$$u(r) = \frac{Q}{2\pi} \frac{\hat{r}}{r} \; . \tag{2}$$

The coefficient of the potential has been rewritten in terms of Q, the areal flux of fluid entering or leaving the system. From Eq. (2), $\oint ds \cdot u(r) = Q$, for any contour enclosing the inner circle once. The initial condition is taken to correspond to a tracer particle initially placed at $r = r_0$. To maintain circular symmetry, this initial condition can be formulated as a ring of tracer particles which are released at $r = r_0$.

$$c(r, t = 0) = \frac{1}{2\pi r_0} \delta(r - r_0) \; .$$

The boundary conditions to be imposed for reflection at $r = R$ and absorption at $r = a$ are $c(a,t) = 0$ and $j(R,t) = 0$, where the radial flux is

$$j(r,t) = -D \partial c(r,t)/\partial r + u(r)c(r,t) \; .$$

For this system, we are interested in the time dependence of the transit probability to the absorbing circle $p(t)$. Because the initial probability density is normalized and all particles that reach the inner circle are absorbed, this transit time probability coincides with the flux at $r = a$, i.e., $p(t) = j(a,t)$. From this connection, we can compute the basic transit time properties of the system.

By introducing the dimensionless radial coordinate $x = r\sqrt{s/D}$ and the Laplace transform $\tilde{c}(r,s) \equiv D \int_0^\infty c(r,t)e^{-st}dt$, the CDE can be written in a standard Bessel form

$$\tilde{c}(x,s)'' - \frac{Pe-1}{x}\tilde{c}(x,s)' - \tilde{c}(x,s) = -\frac{\delta(x-x_0)}{2\pi x_0} \; , \tag{3}$$

with Péclet number $Pe = Q/2\pi D$ and where the prime indicates differentiation with respect to the dimensionless radial coordinate. Details of the Green's function solu-

tion to this equation in an annular geometry are given in Appendix A. From this solution, the Laplace transform of the transit time probability $\bar{p}(s) \equiv \int_0^\infty p(t)e^{-st}dt$ is

$$\bar{p}(s) = \left[\frac{a}{x_0}\right]^\nu \frac{I_\nu(x_0)K_{\nu+1}(R)+K_\nu(x_0)I_{\nu+1}(R)}{I_\nu(a)K_{\nu+1}(R)+K_\nu(a)I_{\nu+1}(R)} . \quad (4)$$

Here I_ν and K_ν are the modified Bessel functions of the first and the second kind, respectively, $\nu = \text{Pe}/2$, and all lengths have been expressed in nondimensional units.

For the inner problem, the transit time probability distribution decays exponentially in time for $R < \infty$. Thus the interesting situation in the long-time limit is that of $R \to \infty$, i.e., the first passage to a small absorbing circle in an infinite system. For this situation, $I_\nu(R)$ diverges with $K_\nu(R)$ vanishes, so that the transit time probability simplifies to

$$\bar{p}(s) = \left[\frac{a}{x_0}\right]^\nu \frac{K_\nu(x_0)}{K_\nu(a)} . \quad (5)$$

To extract the long-time behavior, we need to consider the behavior of $\bar{p}$ as $s \to 0$. Generically, this quantity has a small-s expansion of the form

$$\bar{p}(s) \sim \bar{p}(0) - as^{\alpha_1} + bs^1 + \cdots . \quad (6)$$

By comparison with the definition of the Laplace transform when expanded in powers of s, the zeroth-order term is just the probability $E(r_0)$ that a tracer particle which starts at $r = r_0$ eventually reaches the absorbing circle. That is, $\bar{p}(s=0) = \int_0^\infty p(t)dt \equiv E(r_0)$. If this eventual return probability is unity, the process is recurrent, i.e., the tracer is sure to be absorbed, while if the return probability is less than unity, the process is transient [11]. Additional time-dependent properties can be inferred by the nature of the correction terms in Eq. (6). When the exponent of the first correction term $\alpha_1 < 1$, then the mean transit time diverges and the probability distribution in real time has a power-law tail which varies as $t^{-\alpha_1 - 1}$. However, when α_1 reaches unity, then by comparison again with the formal expansion of the Laplace transform, the coefficient of s coincides with the mean transit time to the absorbing circle, $\langle t \rangle$.

For the transit time probability given in Eq. (5), the first correction to the leading behavior of K_ν, and hence of $\bar{p}(s)$, is generally nonanalytic. This is the source of many of the interesting transit time properties of the system. There are two cases to consider, namely, outward flow $(Q, \nu > 0)$ and inward flow. For outward flow, we use the asymptotic form

$$K_\nu(x) \sim \frac{\pi}{2\sin\pi\nu} \left[\left[\frac{2}{x}\right]^\nu \frac{1}{\Gamma(1-\nu)} - \left[\frac{x}{2}\right]^\nu \frac{1}{\Gamma(1+\nu)} \right. $$
$$\left. + O(x^{2-\nu}) \right] \quad (7)$$

in Eq. (5) to yield, for the transit time probability (now in dimensional units),

$$\bar{p}(s) \sim \left[\frac{a}{x_0}\right]^{2\nu} \left[1 - \frac{\Gamma(1-\nu)}{\Gamma(1+\nu)}(r_0^{2\nu} - a^{2\nu}) \left[\frac{s}{4D}\right]^\nu \right. $$
$$\left. + \cdots \right] . \quad (8)$$

We therefore conclude that the eventual return probability $E(r_0) = (a/r_0)^{2\nu} < 1$. Thus the effect of outward flow is to render a neutral tracer particle transient with respect to a circle of radius a. One way to interpret this result is to notice from Eq. (3) that the outward radial potential flow is equivalent to a purely diffusive system of spatial dimension greater than two. For such a system, it is well known that the probability of eventually hitting a given point (or set of points) is less than unity.

From the correction term in the series for $\bar{p}(s)$, we also deduce that $\langle t \rangle$ diverges for $0 \leq \nu < 1$ (i.e., $0 \leq \text{Pe} < 2$), while for $\nu \geq 1$, $\langle t \rangle$ is finite. Since the eventual return probability is less than unity for $\nu > 0$, $\langle t \rangle$ in this case is conditional on those particles which actually hit the absorbing circle. The situation where $\langle t \rangle < \infty$ but $E(r_0) < 1$ corresponds to strongly transient behavior (which occurs for $d > 4$ in the pure random walk problem). Physically, strong transience simply reflects the fact that for sufficiently large velocity (or, equivalently, for sufficiently large spatial dimension in the case of pure random walks), a tracer particle must reach the absorber in a finite time if it is to be absorbed at all.

For inward flow $(\nu < 0)$, there is a wider range of phenomenology which is evident from the small-s expansion of $\bar{p}(s)$. Using $K_{-\nu} = K_\nu$, we immediately find from Eqs. (5) and (7) that as $s \to 0$, the transit time probability has the expansion

$$\bar{p}(s) \sim 1 - \frac{\Gamma(1-\mu)}{\Gamma(1+\mu)}(r_0^{2\mu} - a^{2\mu}) \left[\frac{s}{4D}\right]^\mu + \cdots , \quad (9)$$

where $\mu \equiv -\nu > 0$. A basic (and not unexpected) feature from this expansion is that $E(r_0) = 1$; a tracer particle hits the absorbing circle with certainty. Additionally for $\mu < 1$, (i.e., $0 \leq -\text{Pe} < 2$), $\langle t \rangle$ is infinite, while for $\mu \geq 1$, $\langle t \rangle$ is finite. Thus even though the tracer is guaranteed to reach the absorber for any inward drift (including zero drift), the transit time is finite only if the drift is sufficiently strong.

The complementary outer problem of a reflecting circle at $r = a$ and an absorbing circle at $r = R$ also leads to interesting behaviors. From Eq. (A14) and the transformation $a \leftrightarrow R$ needed to convert the inner to the outer problem, the transit time probability to the absorbing circle is

$$\bar{p}(s) = \left[\frac{R}{x_0}\right]^\nu \frac{I_\nu(x_0)K_{\nu+1}(a)+K_\nu(x_0)I_{\nu+1}(a)}{I_\nu(R)K_{\nu+1}(a)+K_\nu(R)I_{\nu+1}(a)} . \quad (10)$$

Generically, interesting behavior occurs when the Bessel function K_ν dominates in both the numerator and denominator. This arises because the first correction to the leading behavior of K_ν is generally nonanalytic as its argument goes to zero, while the first correction to I_ν is analytic. Since $K_{\pm\nu}(x)$ both diverge as $x^{-\nu}$ as $x \to 0$, it is

evident that for $v > -\frac{1}{2}$, the first term in both the numerator and the denominator dominate as $s \to 0$ and $\tilde{p}(s)$ reduces to a ratio of I_v's. This leads to a series representation for $\tilde{p}(s)$ which is analytic in s so that the probability decays exponentially in time and the mean transit time is finite. On the other hand, for $v < -\frac{1}{2}$ (i.e., $1 > -\text{Pe}$), the complementary terms dominate in Eq. (10) and as $s \to 0$, $\tilde{p}(s)$ reduces to

$$\tilde{p}(s) \sim \left[\frac{x_0}{R}\right]^{\mu} \frac{K_{\mu}(x_0)}{K_{\mu}(R)} , \tag{11}$$

with $\mu = -v$. This is of the same form as Eq. (5). Thus the probability of eventually reaching the outer circle is unity, while the $p(t)$ has a power-law long-time tail with a velocity-dependent exponent $t^{-\mu-1}$. Physically, this last result indicates that for sufficiently strong inward drift the tendency for concentrating particles near the origin more than compensates for the cutoff in the transit time probability due to the finite extent of the system. Consequently the mean time diverges and there is an attendant power-law tail in the transit time probability.

B. Time integrated properties in d dimensions

For arbitrary spatial dimension d, we have not been able to obtain the analogous Green's function solution as in the two-dimensional case. However, we can determine the properties of the eventual return probability for all d. This is feasible because $E(\mathbf{r})$, the probability of eventually reaching the absorbing set when starting from $\mathbf{r}$, obeys a time-independent equation that can be easily integrated for all d (see, e.g., Ref. [12]). This feature is perhaps best appreciated by considering a discrete hopping process, where $E(\mathbf{r})$ evidently obeys the recursion relation

$$E(\mathbf{r}) = \sum_{\mathbf{r}'} p_{\mathbf{r} \to \mathbf{r}'} E(\mathbf{r}') . \tag{12}$$

Here $p_{\mathbf{r} \to \mathbf{r}'}$ is just the probability of hopping from $\mathbf{r}$ to $\mathbf{r}'$ in a single step. In the continuum limit, this recursion relation becomes $D\nabla^2 E + \mathbf{u} \cdot \nabla E = 0$ and for radial flow simplifies to

$$DE''(r) + \left[D\frac{d-1}{r} + \frac{u_0}{r^{d-1}}\right]E'(r) = 0 . \tag{13}$$

For the illustrative case of absorption at a sphere of radius a in an infinite system $(R \to \infty)$, corresponding to the boundary conditions $E(a) = 1$ and $E(\infty) = 0$ (except for $d < 2$ and $u_0 \leq 0$), the above equation can be integrated by elementary methods to give

$$E(r) = \begin{cases} \dfrac{\exp(\beta r^{2-d}) - 1}{\exp(\beta a^{2-d}) - 1} & \text{for } d > 2 \\[2mm] \exp[\beta(r^{2-d} - a^{2-d})] & \text{for } d < 2 , \ u_0 > 0 \\[2mm] 1 & \text{for } d < 2 , \ u_0 \leq 0 , \end{cases} \tag{14}$$

where $\beta = u_0/D(d-2)$. The qualitative dependence of the eventual return probability on the starting radius is shown in Fig. 1. For $d > 2$, the interesting case is inward
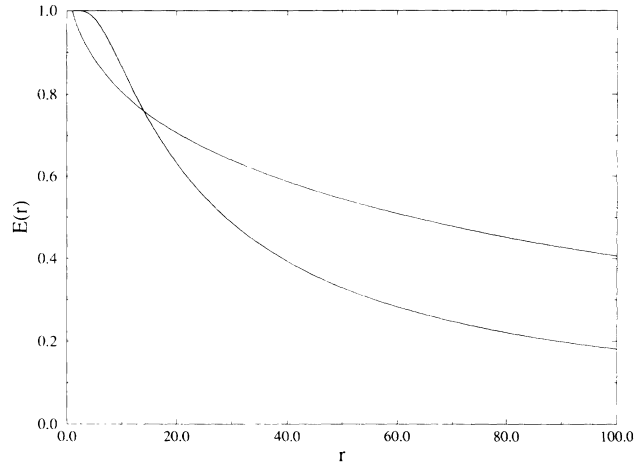

FIG. 1. Schematic dependence of the eventual return probability on the initial radial displacement r_0 for radial potential flow in d dimensions. Shown are the interesting cases of $d > 2$ and inward flow (lower curve for large r) and $d < 2$ and outward flow.

flow, where $E(r)$ remains of order unity for $r < \lambda$ (i.e., $\beta r^{d-2} < 1$) and then drops precipitously to zero for larger r. Related behavior occurs for the case of outward flow for $d < 2$.

III. DIPOLAR FLOWS

We present a full discussion of tracer motion in a two-dimensional dipole flow field, corresponding to a pumping well and a producing well in a thin, circular, homogeneous porous layer. Some of these results have appeared in our earlier paper [13], where the emphasis was on different aspects of the problem. The local tracer concentration $c(\mathbf{r}, t)$ is described by the convection-diffusion equation of Eq. (1), where we assume a constant diffusivity (but see below). Consider a point source and sink placed symmetrically about the center of a circle of radius R, at $\mathbf{r}_{1,2} = (0, \mp a)$, with total flux $\pm Q$. The dipole velocity can be written equivalently as

$$\mathbf{u} = \nabla \phi = \left[\frac{\partial \psi}{\partial y}, -\frac{\partial \psi}{\partial x}\right] , \tag{15}$$

where the velocity potential ϕ and stream function ψ are the real and imaginary parts of the complex potential

$$\Psi = \phi + i\psi = \frac{Q}{2\pi} \ln \frac{(z+a)(z+R^2/a)}{(z-a)(z-R^2/a)} , \tag{16}$$

expressed in terms of $z = x + iy$. In this expression, $\pm R^2/a$ are the locations of the image source and sink needed to make the normal velocity vanish on the circular boundary. The streamlines are plotted in Fig. 2. To avoid singularities, it is sometimes useful to replace the point source and sink by small circles of radius $\epsilon \ll a \ll R$. For large Péclet number, it is natural to assume that the fluid and the tracer are emitted uniformly in angle about the source. (It will be shown below that
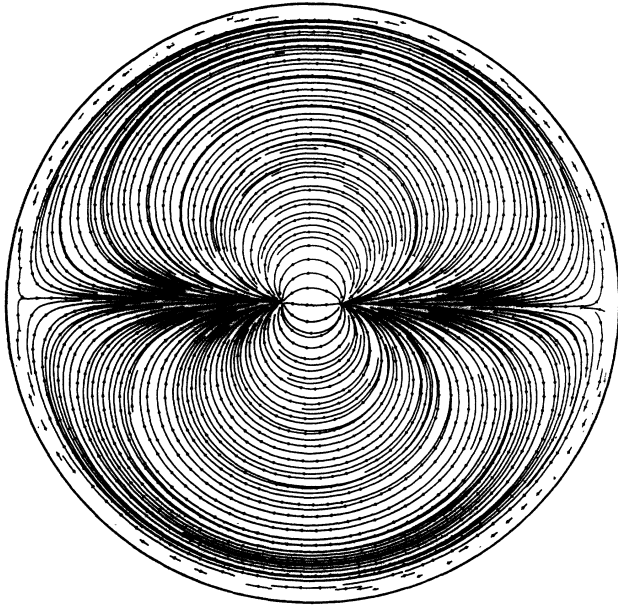
FIG. 2. Streamlines for two-dimensional dipolar flow due to a source at $x = -a$ and an equal strength sink at $x = +a$. The dipole is symmetrically placed inside a circle of radius R. Due to this geometrical constraint, the fluid flow is purely tangential along the circular boundary. Note the existence of the stagnation points at $x = \pm R$.

the time integrated tracer is then also collected uniformly in angle at the sink.) It is convenient to nondimensionalize distance in units of a and time in units of $2\pi a^2/Q$, in which case the coefficient D in the CDE of Eq. (1) is replaced by $Pe^{-1} = 2\pi D/Q$, and $\Psi = \ln\{(z+1)(z+R^2)/[(z-1)(z-R^2)]\}$.

A. The transit time distribution in an ideal dipole flow field

In the limiting case of pure dipolar convection in an infinite plane region ($R \to \infty$), the tracer motion is determined by the velocity field

$$\frac{d\mathbf{r}(t)}{dt} = \mathbf{u}(\mathbf{r}(t)) = \tfrac{1}{2}\nabla \ln \frac{(x+1)^2+y^2}{(x-1)^2+y^2} . \tag{17}$$

In Appendix B we obtain the analytic solution of this problem, using a canonical transformation technique. Mittag and Stephen [14] have independently solved this and related problems using an ingenious conformal transformation method. For a particle emitted at polar angle θ with respect to the source, the transit time to the sink is [Eq. (B6)]

$$t(\theta) = 2\csc^2(\theta)[1 - \theta\cot\theta] \underset{\theta \to \pi}{\to} \frac{2\pi}{(\pi-\theta)^3} . \tag{18}$$

Although the motion is completely deterministic, a distribution in the transit time results from the distribution in the initial angle. Since all streamlines lead from the source to the sink, there is a one-to-one equivalence between the time dependence and angular dependence of the transit time probability. This leads to the probability

that the tracer is collected at time t, which varies as

$$p(t) = p(\theta)\left|\frac{d\theta}{dt}\right| = \frac{1}{2\pi t'(\theta)} \underset{\theta \to \pi}{\to} \tfrac{1}{3}(2\pi)^{-2/3} t^{-4/3} . \tag{19}$$

In Eqs. (18) and (19) we emphasize the limiting long-time behavior associated with tracer particles which initially move away from the sink. It is this aspect of the distribution that explores the global structure of the flow field and will be seen to have generic behavior. In contrast, the early arrival component of the distribution obviously involves specific geometric features, such as the precise source-sink separation. Note that the $t^{-4/3}$ tail of the distribution implies that the mean transit time $\langle t \rangle = \int_0^\infty dt\, t p(t)$ diverges, as expected for an infinite volume system.

In the opposite limit of pure diffusion in an infinite volume, the transit time distribution can be computed exactly by a variety of approaches. For a source and a sink that are a finite distance apart, $p(t)$ asymptotically varies as $1/(t\ln^2 t)$, independently of the distance between the two sites. The behavior can be easily obtained from our earlier treatment of radial flow in an annulus. If we consider the sink to be the small circle of radius a and take the limit where the outer radius is infinite, then for zero flow the transit time distribution is simply given by Eq. (5) with $v=0$. As $s \to 0$, the limiting behavior is $\tilde{p}(s) \sim 1 + \text{const}/\ln s$. In the time domain, this corresponds to a probability distribution that varies as $1/(t\ln^2 t)$. Although this asymptotic estimate is based on a system with an initial circular distribution of the tracer, it obviously applies to the case of a point source of the tracer. (Indeed, in the point-source case, the initial condition would require a Fourier series in $e^{in\theta}$, but the long-time behavior would be controlled by the $n=0$ term, and moreover the $n \neq 0$ terms would not contribute to the integral over all angles.) For such a transit time distribution, all of the tracer eventually reaches the sink, but the mean time to diffuse from the source to the sink diverges. If, however, the linear dimension R of the system is finite, then the transit time distribution exhibits an exponential cutoff with a time constant proportional to R^2/D (in physical units), the time to diffuse across the system.

B. Numerical results and their interpretation

For situations more complex than a dipole in an infinite medium or pure diffusion, further progress by analytical techniques does not appear possible and we therefore turn to numerical methods. For example, for a dipole with pure convection in a finite domain, the canonical transformation technique becomes intractable. To determine the transit time distribution, we numerically integrate $d\mathbf{r}/dt = \mathbf{u}$, using the full potential Eq. (16), with $R = 100$ (Fig. 3). This calculation yields the expected $t^{-4/3}$ power-law tail over a substantial temporal region, but eventually an exponential decay $p(t) \sim e^{-t/t_c}$ sets in. In [13], it was shown that the decay constant can be related to the nature of the flow in the vicinity of the two stagnation points at $\mathbf{r} = (\pm R, 0)$ and has the value

$t_c = R^3/2 - 3R/2 + \cdots$ in the present dimensionless units. The value $t_c \approx 5 \times 10^5$ deduced from the figure agrees with this calculation.

In fact, it is easy to show that stagnation points in general flows lead to an exponential decay in the transit time distribution. Without loss of generality, consider a stagnation point at the origin in which the velocity has the local form $\mathbf{u} = d\mathbf{r}/dt = (-Gx, Gy)$. If the stagnation point is approached along the x axis, then trajectories which pass near the origin and then escape have the form $\mathbf{r}(t) = (x_0 e^{-Gt}, y_0 e^{Gt})$ with $y_0 \ll x_0$. The time T spent near the stagnation point can be defined by requiring that $\dot{y} \sim U_0$, where U_0 is some characteristic $O(1)$ velocity.

(a)

$p(t)$ vs t

(b)

$p(t)$ vs t
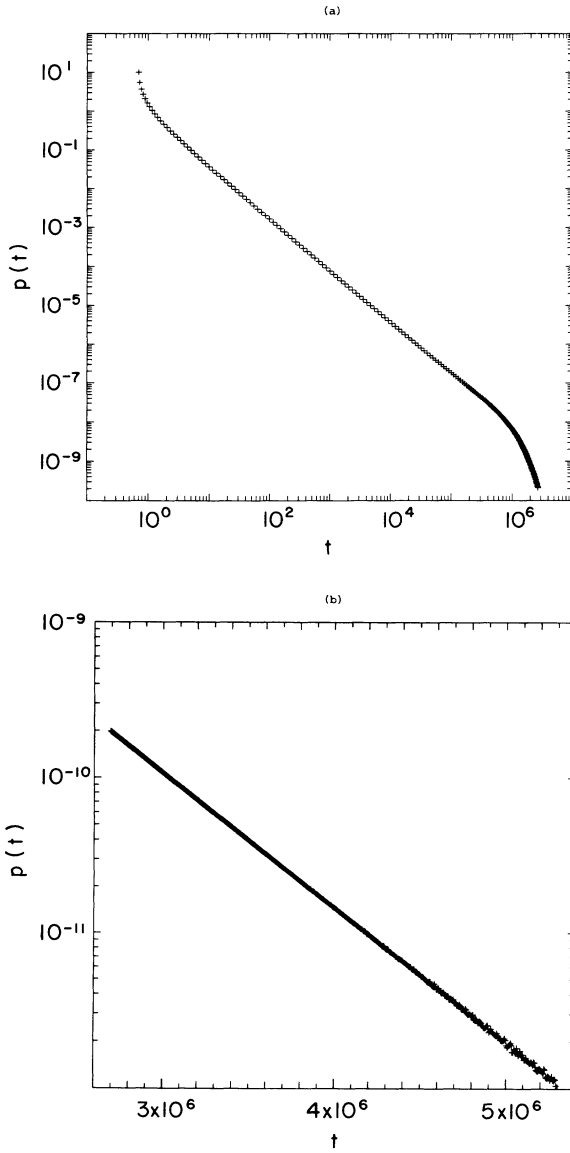
FIG. 3. Transit time probability distribution for the tracer in the convective limit for dipolar flow with the source and the sink at $x = \mp 1$ inside a circle of radius $R = 100$. (a) In the regime where the decay is a power law, a straight-line fit to the data yields the exponent estimate of -1.33. (b) The exponential decay in a semilog plot, with decay constant 5×10^5.

Since $\dot{y} \sim y_0 Ge^{GT}$, this gives $T \sim G^{-1}\ln(U_0/y_0 G)$. Typically, for trajectories that pass near a stagnation point, the transit time between the source and the sink is dominated by this value of T. The corresponding distribution of transit times may now be obtained by accounting for the distribution of initial positions y_0. Consequently,

$$p(T) = p_0(y_0) \left| \frac{dy_0}{dT} \right| = p_0 \left[\frac{U}{G} e^{-GT} \right] \left| -Ue^{-GT} \right|$$

$$\underset{T \to \infty}{\sim} p_0(0)e^{-GT} . \tag{20}$$

Thus the transit time distribution depends on the local shear rate near the stagnation point, but not on the details of the initial spatial distribution of the tracer p_0. In the present case of a dipole placed at the center of a circle, the strain rates at the stagnation points at $(\pm R, 0)$ may be computed from Eqs. (15) and (16) to be

$$G = \left| \frac{\partial u}{\partial r}(\pm R, 0) \right| = \frac{4}{R^3} \frac{(1 + 1/R^2)}{(1 - 1/R^2)^2} . \tag{21}$$

Since tracer particles that are emitted close to $\theta = \pi$ encounter two stagnation points, the cutoff time constant is twice G^{-1}, or $p(t) \sim e^{-Gt/2}$, in agreement with [13].

For the general case of finite radius and finite Péclet number, we turn to the numerical simulation of the CDE. The simplest method is a grid-free Monte Carlo time-stepping procedure using individual random walkers. In time Δt, a walker is displaced by

$$\Delta \mathbf{r} = \mathbf{u}(\mathbf{r})\Delta t + \hat{\mathbf{n}}(4\Delta t/\mathrm{Pe})^{1/2} , \tag{22}$$

where $\hat{\mathbf{n}}$ is a unit vector of random orientation. The time step interval may be chosen at each point on the trajectory to ensure that individual displacements are less than a suitable bound, so that there are no pathologies associated with the large velocities near the source and the sink. On the other hand, significant diffusion leads to substantial statistical fluctuation in the results. Figure 4 gives a typical result for specific parameters relevant to our previous paper [13]: $a = 1$ cm, $R = 11$ cm, $D = 10^{-5}$ cm^2 s^{-1}, $Q = 0.17$ cm^2 s^{-1}, leading to Pe $= 2700$, and $N = 500\,000$ random walkers. In the figure there is an early time peak, followed by the anticipated $t^{-4/3}$ power-law region, followed by a noisy region, which perhaps exhibits a shoulder and then an exponential decay. In principle, the noise could be reduced by considering more walkers, but such fluctuations only decay as $N^{-1/2}$ and more systematic methods are preferable (see below).

We have also used this single-random-walker method to verify that the power-law tail is not sensitive to the effects of "convective" dispersion, namely, the enhancement of the diffusivity due to convective pore-scale mixing mechanisms which occur in porous media flows [4,5]. We adopt the simple parametrization

$$D_\parallel = D[1 + \mathrm{Pe}'] , \quad D_\perp = D[1 + \mathrm{Pe}'/10] , \tag{23}$$

which approximately fits the accumulated experimental data on sandstones [10]. Here the diffusion tensor is diagonal with distinct components parallel and perpendicu-
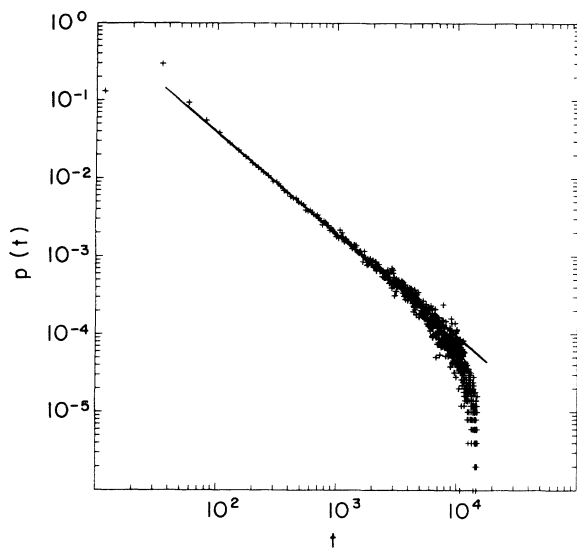

FIG. 4. Transit time probability distribution in the combined dipolar flow and molecular diffusion. Simulation of the diffusion is accomplished by following the motion of individual random walks in the background flow field. For this system, the Péclet number Pe = 2700.

lar to the flow, D is the molecular diffusivity, and Pe′ is a pore-scale Péclet number defined as ud_g/D, with d_g the grain diameter and u the *local* velocity. In applying Eq. (22), the factor D in Pe^{-1} is replaced by the projection of Eq. (23) along the direction of the diffusive step. Using the same parameters as in the previous case of constant diffusivity and $d_g = 0.025$ cm, we find a transit time distribution statistically indistinguishable from Fig. 4, except for somewhat more noise in the tail region. The basic reason we see no effect is that the convective enhancement of the diffusivity is proportional to Péclet number, so that at low Pe′ the enhancement is absent, while at high Pe′, where it is an appreciable correction to the diffusivity, the tracer motion is dominated by convec-

vection anyway. In view of this insensitivity, we neglect convection dispersion in the rest of this paper.

To resolve the effects of diffusion in the tail region, we treat directly the ensemble of random walkers or, equivalently, the continuum concentration field. We have employed two finite difference algorithms which give the same results. One procedure is simply a "probability propagation" method, in which initially there is a unit probability to be at the source, and at subsequent times the distribution convects and diffuses to an average position which is, in general, off the lattice. This continuum spreading is replaced by motion to a discrete five-site neighborhood such that the mean position and the dispersion of the discrete motion about the average coincides with that of the true continuum motion. This algorithm complements the single-walker method by focusing on the full probability distribution, whose support eventually grows to encompass the whole system, rather than a single walker at a specific location. Details of the algorithm are given in Appendix C.

To test the validity of the probability propagation method, we reconsider the exactly solved case of radial potential flow within a two-dimensional annulus. The time dependence of the transit time probability distribution for inward flow when $a = 1$, $r_0 = 10$, and $R = 80$ and an initial localized ring of the tracer at $r = r_0$ is shown in Fig. 5. After a peak associated with tracer which reaches the sink directly, there follows a temporal regime where $p(t)$ decays as a power law in t. The power-law regime in Fig. 5 terminates in a shoulder which occurs when the time comparable to the diffusion time across the system $t_d = O(R^2 Pe)$. Our interpretation of this feature is that it results from the tracer, which diffuses away from the sink and *rebounds* from the outer boundary before diffusing and convecting back to the sink for collection. To reinforce this claim, we consider an analogous and exactly soluble one-dimensional situation, where a similar effect arises (Appendix D). Beyond the shoulder, the transit time distribution decays exponentially, with a time constant proportional to the diffusion time $t_d = O(R^2 Pe)$.

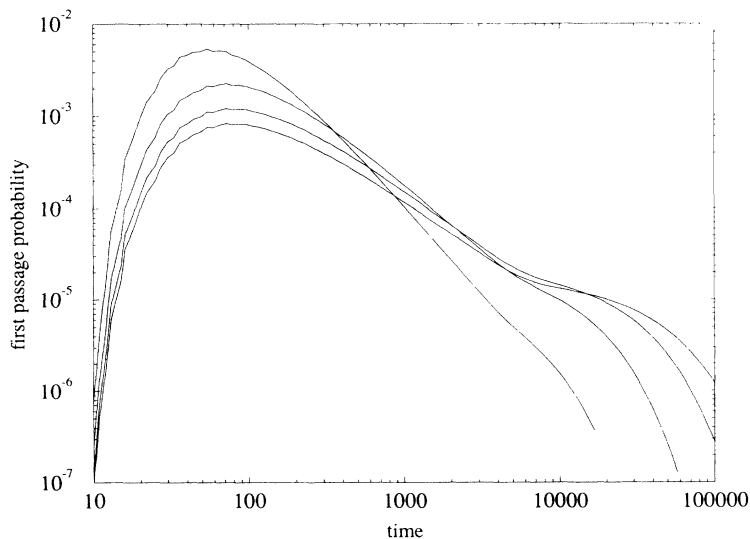A noteworthy feature of the transit time distribution is

FIG. 5. Transit time probability distribution, using the probability propagation method, in combined radial flow and diffusion within an annulus of outer radius $R = 80$ with the initial probability uniformly distributed within a ring of radius $9.5 < r_0 < 10.5$. The absorber consists of a single site at the origin. Shown are the distributions for the representative set of Péclet numbers Pe = 2, 1, $\frac{1}{2}$, and $\frac{1}{4}$ (narrowest to broadest peak, respectively).

that the exponent of $p(t)$ appears to depend on the Péclet number, as anticipated from the analytic solution. To estimate this exponent numerically, we examine the local exponents, which are defined as the slopes between adjacent points in the double logarithmic plot. (For a systematic analysis of these local exponents, it is essential to take data at equally spaced points on a logarithmic time scale). Plotting this local exponent versus $1/t$ reveals a substantial time range where the exponent is slowly varying in time and a confident extrapolation to $1/t \to 0$ can be performed. As shown in Fig. 6, the extrapolated value of the local exponent for different values of Pe are in excellent agreement with the analytic predictions. This provides confidence that the simulation approach and attendant analysis methods will provide useful quantitative information when applied to more complicated flows.

We now turn to the simulation results for combined dipolar flow and diffusion inside a finite circle based on the probability propagation method (Fig. 7). The transit time distribution exhibits the same four qualitative regimes of behavior as observed in radial flow. Additionally, as in radial flow, the exponent of $p(t)$ appears to depend on the Péclet number in the power-law regime. This is in contrast to the pure-convection calculations and single-walker simulations at large values of Pe, which both indicate a temporal region where $p(t)$ decays as $t^{-4/3}$, when starting with an initial tracer pulse. To clarify the meaning of this apparent Péclet-number-dependent exponent for $p(t)$, we reexamine the local exponent in the data for $p(t)$. In the temporal range where power-law behavior seems to occur $(5000 \lesssim t \lesssim 50\,000)$, the local slope changes slowly with time and appears to extrapolate to a value close to -1.3 for several different values of Pe (Fig. 8). This asymptotic value appears to be more plausible for data with Péclet numbers near the upper limit of validity of the simulation method. For smaller values of Pe, the asymptotic exponent associated with $p(t)$ does appear to be larger than $-\frac{4}{3}$. Since $p(t) \sim 1/(t \ln^2 t)$ in the diffusive limit and $p(t) \sim t^{-4/3}$ as $Pe \to \infty$, it seems unlikely that a simulation method that cannot be applied at large Pe will be able to resolve these two limiting

behaviors clearly. Nevertheless, the extrapolations of the local exponents are suggestive of a universal behavior in the tail of $p(t)$.

As a further check on the probability propagation results, we have considered an alternative numerical treatment based on a conformal transformation of the CDE. This approach provides a considerable geometrical simplification, which is useful in other contexts. Thus consider conformally transforming the flow domain from (x,y) into (ϕ,ψ) coordinates. In the latter variables, the CDE becomes

$$|\mathbf{u}(\phi,\psi)|^{-2}\frac{\partial c}{\partial t} + \frac{\partial c}{\partial \phi} = \frac{1}{Pe}\left[\frac{\partial^2 c}{\partial \phi^2} + \frac{\partial^2 c}{\partial \psi^2}\right]. \qquad (24)$$

That is, the curvilinear flow is transformed to linear flow by using the complex potential as the conformal transform, but at the expense of introducing a spatially dependent time step which is singular as $(0, i\pi)$ is approached. Furthermore, if we simplify by taking the $R \to \infty$ limit of Eq. (16), the flow domain is a rectangle bounded by the source and the sink located at $\phi = \pm \ln(\frac{1}{2}\epsilon)$, respectively, with the direct path from the source to the sink on the x axis mapped into $\psi = 0$ and the remainder of the x axis plus the point at infinity mapped into $\psi = \pi$. The numerical solution of Eq. (24) is carried out using centered differencing in space and explicit time stepping. Aside from the usual numerical checks of varying the grid and time spacing, we verify that the amount of tracer lost from the system $1 - \int |\mathbf{u}|^2 c \, d\phi \, d\psi$ equals the time integral of the outgoing flux. Some typical numerical results of this method for $Pe = 0.5 - 10$ are shown in Fig. 9, which is in general agreement with the results of probability propagation. This finite difference method also exhibits an exponent that appears to depend on Pe. As the Péclet number becomes large, the finite difference approach requires a fine grid for accuracy, especially in the high-velocity regions, which in turn requires an extensive computation. One could overcome these technical difficulties by using a suitable variable-sized grid, but our
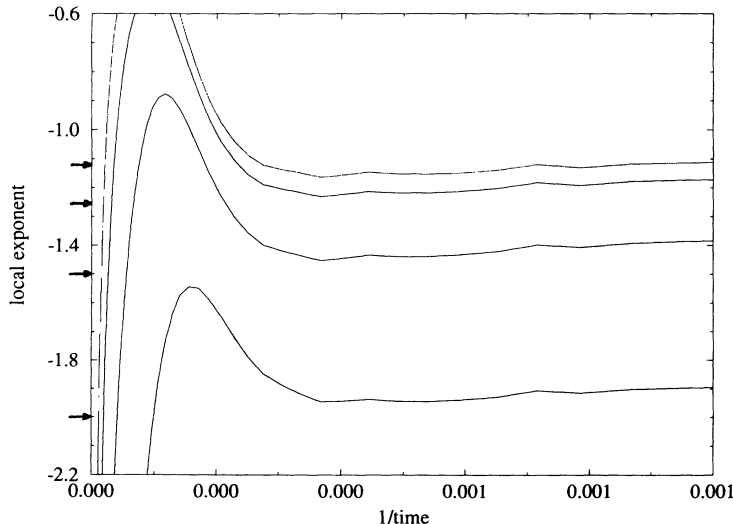
FIG. 6. The local exponent of the transit time distribution (based on slopes of successive points in the preceding figure) plotted vs $1/t$. Lower to upper curves correspond to decreasing values of Pe. The local exponent appears to extrapolate to the expected asymptotic value of $-1-(Pe/2)$ (arrows) before the trend is interrupted by the sharp rise and rapid decrease in the local exponent due to the finite-size rebound shoulder and the ultimate finite-size exponential decay.
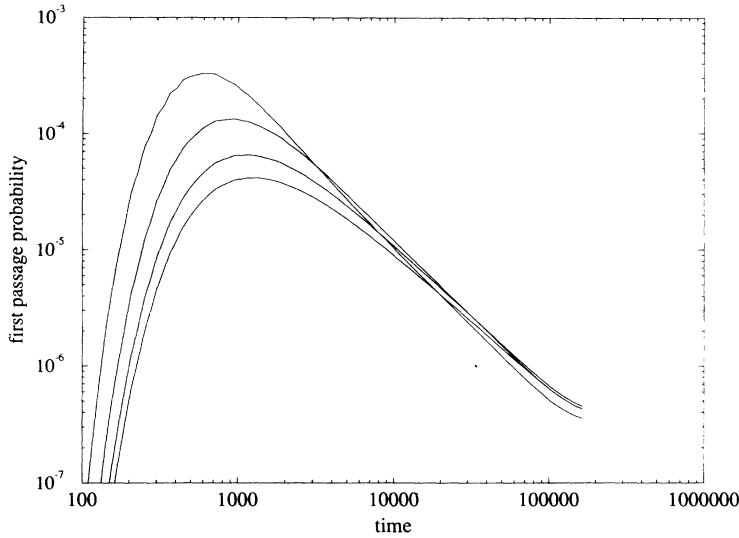
FIG. 7. Transit time probability distribution in combined dipolar flow and diffusion within a circle of radium $R = 400$ with the source and the sink at $x = \mp 20$ using the probability propagation method shown are the distributions for the representative set of Péclet numbers Pe $= 1.6, 0.8, 0.4$, and 0.2 (tallest to shortest peak, respectively).

purpose here is to explore general features for a variety of flow configurations, without resorting to delicate numerical algorithms.

To summarize, for combined dipolar convection and diffusion in a finite circle, the key features of the transit time distribution are as follows.

(i) *Early time regime.* The transit time distribution rapidly rises to a peak shortly after particles that follow a direct trajectory first reach the sink. In this and the other flows considered below, the early time behavior depends on the specific geometry of the flow domain and there are no general system-independent features.

(ii) *Power-law tail.* After the peak, the transit time distribution falls as a power of t, with an exponent that appears to depend on the Péclet number, but tends to the pure-convection value of $\frac{4}{3}$ as Pe increases.

(iii) *Rebound shoulder.* A shoulder appears in the transit time distribution at times comparable to the diffusion time across the system $t_d \sim R^2 \mathrm{Pe}$ (R^2/D in physical units).

(iv) *Asymptotic decay.* The transit time distribution de-

cays exponentially, with a time constant given by the smaller of the diffusive value $t_d = O(R^2 \mathrm{Pe})$ or the convective value $t_c = R^3/2$.

Similar regimes of behavior also characterize the qualitative features of the transit time distribution for radial flow in an annulus. The experiments discussed in our earlier paper [13] observed the power-law regime and the beginnings of a cutoff, but did not have sufficient resolution at small values of tracer concentration to observe the shoulder or determine the exponential decay constant.

C. Orientation distribution of the collected tracer

We have discussed the transit time distribution of a tracer that reaches the sink without regard for the direction of arrival or, equivalently, *where* on the sink the tracer was collected. Such directional information might provide a refined diagnostic tool about a tracer that samples specific regions of the pore space and flow field. We now demonstrate that for a passive tracer that is uniformly released in a steady potential flow between a
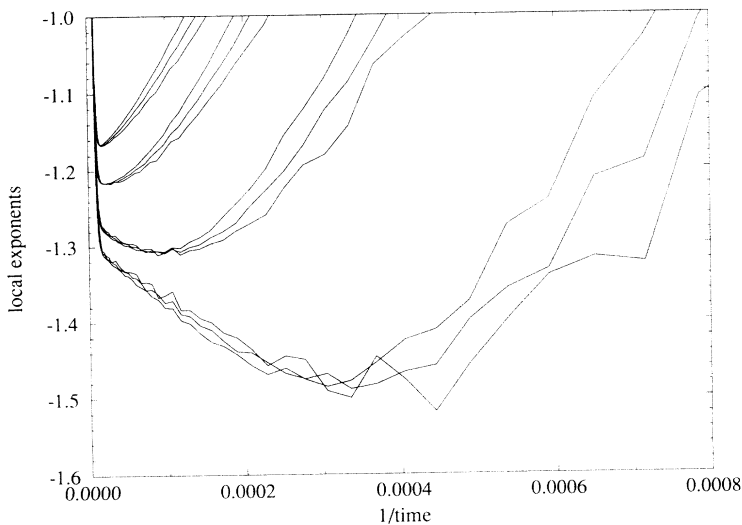

FIG. 8. The local exponent of the transit time distribution, based on slopes of successive second-neighbor, fourth-neighbor, and sixth-neighbor points in Fig. 7, plotted vs $1/t$. Lower to upper curves correspond to decreasing values of Pe. The time range for which power-law behavior occurs is $t \gtrsim 2000$. For the largest Péclet number simulated, the local exponent appears to extrapolate to value close to $-\frac{4}{3}$, before the trend is interrupted by the sharp rise in the local exponent due to the finite-size rebound shoulder.
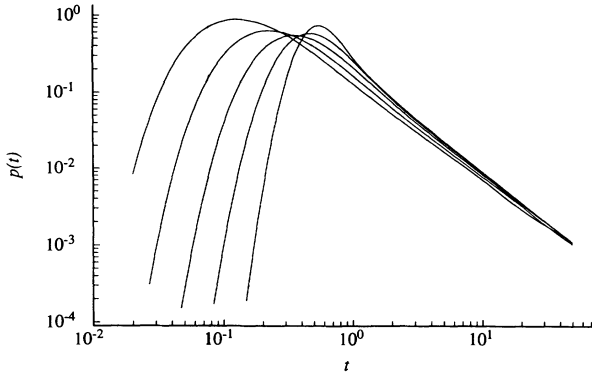
FIG. 9. Transit time probability distribution in dipole flow using the finite difference method, Pe = 0.5, 1.0, 2.0, 4.0, and 10.0, respectively, for curves whose starting points run from left to right.

source and a spatially extended equipotential sink, the time integrated tracer flux distribution at a given point on the sink is simply proportional to the incoming fluid velocity at this point, independent of Pe. (Note that the assumption of a uniform tracer flux at the source is extremely accurate if the source is nearly pointlike, as it often is in practice, for then the fluid velocity is radially outward and large at the source and the tracer simply convects with the fluid.) By the linearity of the transport problem, this theorem implies that the spatial distribution of the collected tracer is *independent* of the overall magnitude of the flow. While this implies that the relative accumulation of a tracer at different points along the sink does not provide a useful diagnostic tool for the flow field, a general equivalence between tracer distributions for pure diffusion and for situations with both convection and diffusion is established.

To prove the theorem, we begin with the CDE written in (ϕ,ψ) coordinates in Eq. (24) and define $\xi(\phi,\psi)=\int_0^\infty dt\, c(t,\phi,\psi)$. The source is taken to be $\phi=\phi_0$, and if the initial condition is that a δ-function pulse of a tracer is injected at the source, then in the equation of motion for ξ the time derivative term integrates to zero, yielding

$$\text{Pe}\frac{\partial\xi}{\partial\phi}=\frac{\partial^2\xi}{\partial\phi^2}+\frac{\partial^2\xi}{\partial\psi^2}\ ,\tag{25}$$

with boundary conditions $(1-\text{Pe}^{-1}\partial/\partial\phi)\xi=K$ at $\phi-\phi_0$, where K is a Pe-independent constant, and $\xi=0$ at $\phi=\phi_1$. The solution of Eq. (25) is

$$\xi=K(1-e^{\text{Pe}(\phi-\phi_1)})\tag{26}$$

and the time integrated tracer flux arriving at the sink is

$$p(\psi)\equiv\int_0^\infty dt\, p(t,\psi)=-\text{Pe}^{-1}\int_0^\infty dt\frac{\partial c}{\partial n}(\phi_1,\psi,t)$$

$$=-\text{Pe}^{-1}\frac{\partial\xi}{\partial n}(\phi_1,\psi)$$

$$=-\text{Pe}^{-1}\frac{\partial\xi}{\partial\phi}\frac{\partial\phi}{\partial n}\bigg|_{(\phi_1,\psi)}\ ,\tag{27}$$

where $\hat{n}$ refers to the direction normal to the sink. In the last expression in (27), the first derivative is a constant and the second is simply the normal velocity of fluid at the sink. Hence

$$p(\psi)\propto u_n(\psi)\ ,\tag{28}$$

as claimed.

Notice that the theorem also holds in the pure diffusion limit, as can be seen by taking Pe→0 either in the equation for ξ or in its solution. In this case, the appropriate statement is that $p(\psi)$ is constant for a constant arc length of the sink. Conversely in the limit of no diffusion the theorem is obvious, because then tracer particles remain on their initial streamline and the tracer flux is simply proportional to the fluid flux. The nontrivial implication is that in the presence of combined convection and diffusion, the local flux is unchanged. Thus, in simple dipole flow, the time integrated flux at the sink is independent of the arriving angle and the Péclet number, although the transient flux depends on both. Unfortunately, the proof does not readily generalize to multiple sources and sinks, because each of these would be associated with different values of ψ (i.e., a particular source-sink pair is connected by a certain group of streamlines, corresponding to a limited range of ψ), and the solution of Eq. (25) cannot be written trivially as a function of ϕ alone.

IV. MORE GENERAL FLOW CONFIGURATIONS

We have seen that simple dipole flows are characterized by a region of power-law decay of the transit time distribution $p(t)\sim t^{-n}$, with $n=\frac{4}{3}$. In this section we consider more complicated flows and again obtain power-law decays, but in general with different values of the exponent n. It is easily seen, however, that the value of n is constrained to lie between 1 and 2. First, note that all of the tracer eventually reaches the sink, because two-dimensional diffusion is recurrent and the additional convection always directs the tracer toward the sink and so $\int_0^\infty p(t)dt=1$. Next, recall that the asymptotic power-law decay would apply for $t\to\infty$ in an *infinite* system and there, as mentioned in the Introduction, the mean first-passage time necessarily diverges: $\int_0^\infty tp(t)dt=\infty$. The two integral constraints imply $1<n<2$.

A. Nonsymmetric dipole flows

We first consider more general flows which originate from multiple point sources or sinks, but where the velocity potential still has a nonzero dipole moment. The simplest possibility, which also provides a substantive application of the orientation theorem Eq. (28), is that of a

point source in the presence of an infinite line sink along the y axis where the velocity potential $\phi=0$. This is essentially "half" the dipole problem. Correspondingly, the streamlines resemble those in the left half of Fig. 2, the angle-dependent transit times are half those of Eq. (18) in the convective limit, and the transit time distribution has the same shape as that of the ideal dipole, except that the time scale is halved.

The information provided by the orientation theorem in this case is that spatial distribution of tracer on the y axis is proportional to the normal velocity $u(0,y)=2/(1+y^2)$. It is straightforward to verify this

result directly from the trajectories in the pure-convection limit. Using the particle trajectories given by Eq. (B3) for an infinite system, for $x=0$ and $\epsilon\to0$, we have $\tan\theta(x=0,y)=2y/(1-y^2)$. Thus the relevant probability distribution function is

$$p(y)=p(\theta)\left|\frac{d\theta}{dy}\right|=\frac{1}{\pi}\frac{1}{1+y^2}=\frac{1}{2\pi}u(0,y) , \qquad (29)$$

as required by the orientation theorem. This same result holds in the complementary case of no convection, as can be checked explicitly. For pure diffusion, the particle
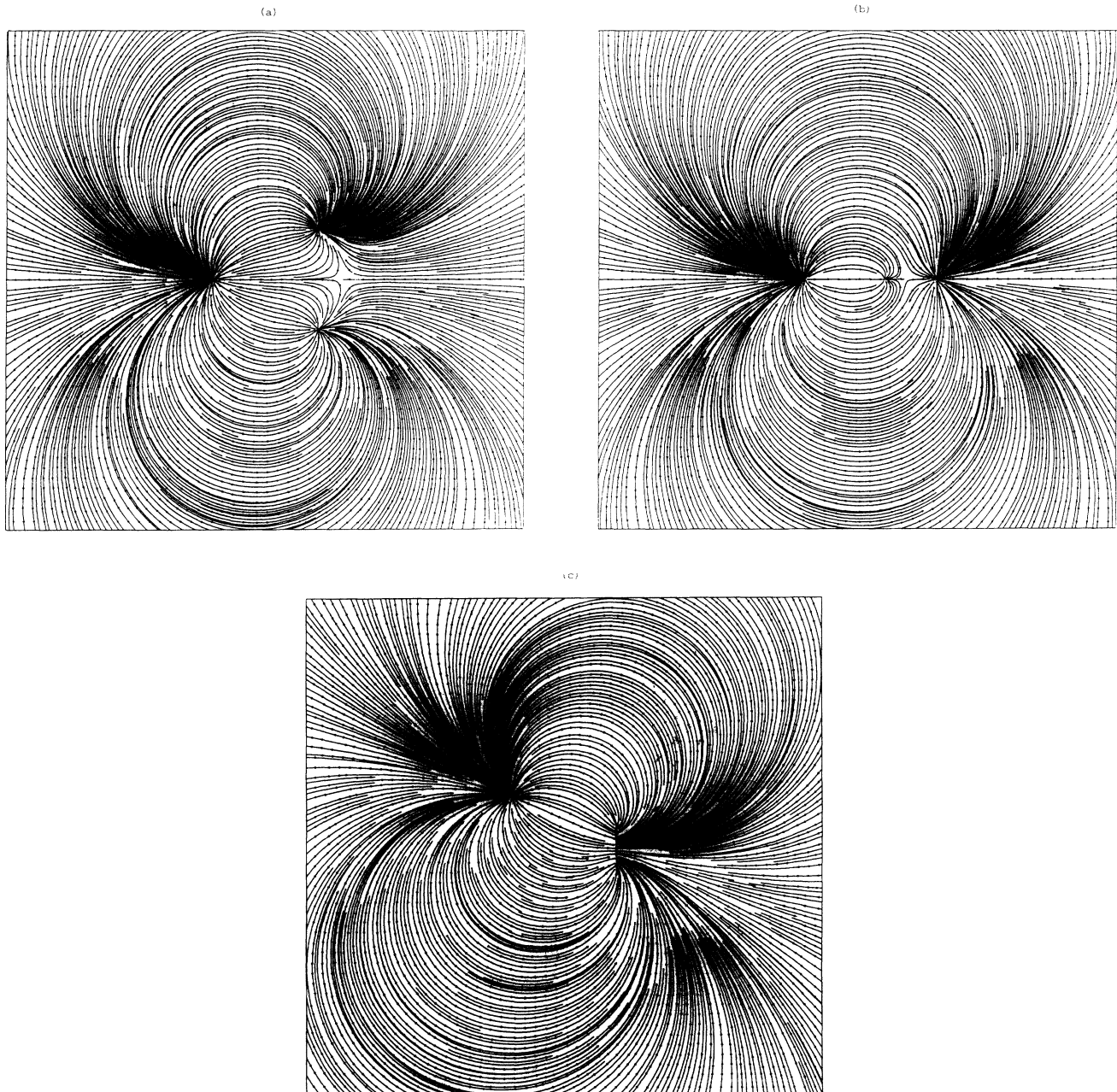
FIG. 10. Streamlines for modified dipole flow configurations: (a) a source and two sinks, each symmetrically displaced in the y direction; (b) a source and two sinks, both on the x axis; and (c) a source and a finite line sink.

concentration is given by

$$c(x,y,t) = \frac{1}{4\pi Dt} \{ e^{-[(x-a)^2+y^2]/4Dt}$$

$$-e^{-[(x+a)^2+y^2]/4Dt} \} , \qquad (30)$$

from which the time-dependent flux at lateral position y along the sink is

$$j(x=0,y,t) = -D \frac{\partial c(x,y,t)}{\partial x} \bigg|_{y=0}$$

$$= \frac{a}{4\pi Dt^2} e^{-(a^2+y^2)/4Dt} . \qquad (31)$$

By integrating this expression over all time, we again obtain Eq. (29). In fact, this equivalence for pure convection and pure diffusion, together with numerical observa-
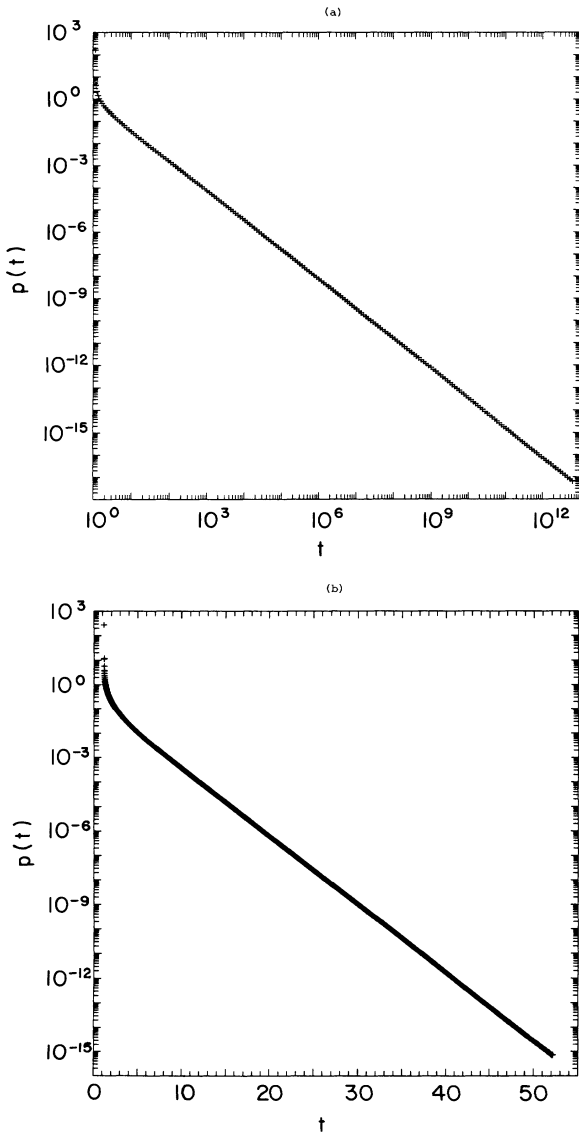

(a)

(b)

FIG. 11. Transit time probability distribution in the convective limit for the flow of Fig. 10(a): (a) trajectories emanating from $\theta \approx 0$ and (b) trajectories emanating from $\theta \approx \pi$.

tions of this same spatial distribution for combined diffusion and convection, led us to the theorem. This system provides a striking illustration that the time integrated spatial distribution of the tracer is velocity independent.

More generally, we have considered the tracer transit time distribution for representative dipolar flows given in Fig. 10. We restrict our analysis of these cases to the pure-convection limit in an infinite domain. Based on the results of Sec. III, the inclusion of diffusion does not alter the interesting and universal power-law regime of behavior for the transit time distribution. For simplicity, first consider a point source and two point sinks at symmetric lateral positions [Fig. 10(a)]. The resulting streamline pattern exhibits a characteristic dipolar form at large distances from the source and the sinks and a stagnation point roughly between the two sinks. The transit time distribution in Fig. 11 reflects these two features. The $t^{-4/3}$ power-law tail in $p(t)$ is associated with the streamlines that are directed away from the stagnation point and the exponential decay of $p(t)$ stems from tracer particles that are initially directed toward the stagnation point. (Note that the power-law behavior will dominate an integral over angles.) The power-law behavior is universal because in all of these cases, at large distances from the source-sink region, the streamlines are indistinguishable from those of a pure dipole. Thus, except for a small fixed correction associated with the near-field region, the trajectories and transit times are the same as a pure dipole. A more quantitative argument along these lines will be presented below in connection with higher multipole flows.

An example of flow with a point source and finite-length line sink is shown in Fig. 10(c). The flow field in the vicinity of the source and the sink differs from that in the previous example in that there are no stagnation points, although the overall flow is dipolar at large distances. The resulting transit time distribution shows the generic early time peak and the $t^{-4/3}$ tail. With multiple line sinks or with multiple sources, stagnation points and their resulting exponential behavior would again occur. For general patterns of sources and sinks, either pointlike or extended, it is evident from this discussion that one would find both power-law and possibly exponential decay regimes for the transit time distribution, *provided* that there is a net dipole moment in the flow.

B. Quadrupolar flows

Higher multipole flows leads to a power-law decay for the transit time distribution, which is characterized by an exponent that is different from that in the dipolar case. Consider, for example, quadrupole flow, arising from a source of flux $2Q$ at the origin and sinks of flux $-Q$ each at $x = \pm a$ (Fig. 12). The resulting transit time distribution in the convective limit, obtained by integrating $d\mathbf{r}/dt = \mathbf{u}(\mathbf{r})$, is given in Fig. 13. In this case, $p(t)$ clearly decays as $t^{-3/2}$ over nearly the entire time range, in accord with a prediction for flows of arbitrary multipolarity, which will be derived in Sec. IV C.

The corresponding distribution for combined convec-
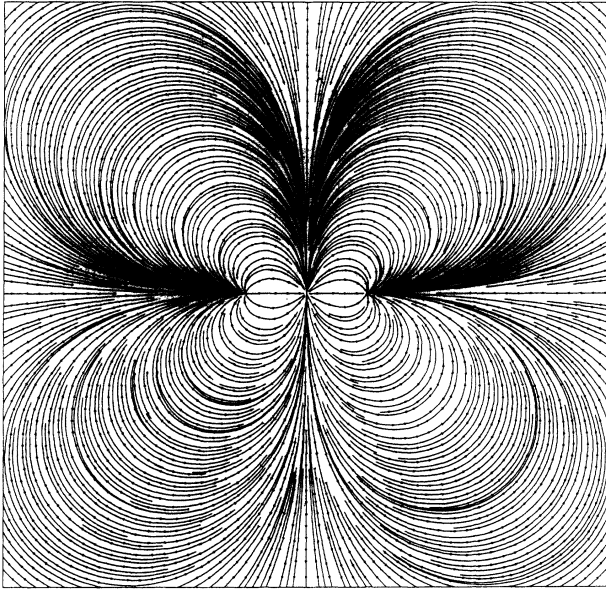
FIG. 12. Streamlines for quadrupolar flow.

tion and diffusion for various values of Pe, obtained by probability propagation, is shown in Fig. 14 When both convection and diffusion are operative, time reversal symmetry of the trajectories is broken and two situations may be considered: (a) the quadrupole, which consists of point singularities of strength $(-Q, 2Q, -Q)$ located at $(-a, 0, a)$, and (b) the "inverted" quadrupole, which consists of point singularities of strength $(Q, -2Q, Q)$ located at $(-a, 0, a)$. The qualitative appearance of the transit time distributions for these two situations with the same value of the Péclet number is quite different. Following the same analysis protocol as in the dipolar case, it is seen that in the quadrupole system the transit time probability appears to decay as $t^{-1.2}$ over a substantial time range [Fig. 15(a)]. For the inverted quadrupole, on the other
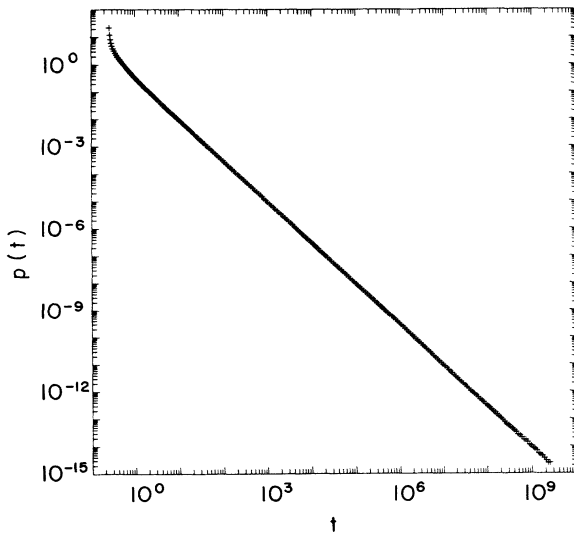
FIG. 13. Transit time probability distribution in the convective limit for quadrupolar flow.

hand, the exponent of $p(t)$ appears to depend on the Péclet number [Fig. 15(b)]. The apparent nonuniversality is evident in the graphs of $p(t)$ themselves. The dichotomy in the behavior of the two types of quadrupoles is as yet unexplained.

C. Flows of arbitrary multipolarity

The quadrupolar results suggest consideration of the transit time distribution for a source-sink of arbitrary multipolarity. We present here a simple argument that relates the exponents of the transit time distribution to order of the multiple moment. For an arbitrary distribution of sources and sinks $q(\mathbf{r})$, the *two-dimensional* multipole expansion of the complex potential is

$$\Psi(z) = \frac{1}{2\pi} \int d^2 z' q(z') \ln(z - z')$$

$$= \frac{1}{2\pi} \int d^2 z' q(z') \left[\ln z - \sum_{n=1}^{\infty} \frac{1}{n} \left(\frac{z'}{z} \right)^n \right], \quad (32)$$

where $z = x + iy$ and similarly for z'. For a 2^N pole, the leading nonvanishing term in the multipole expansion is $n = N$. Therefore $\Psi \sim z^{-N}$ and the corresponding streamlines are $\psi = \mathrm{Im}\Psi \sim r^{-N}\sin(N\theta)$, for a suitable orientation of the axes. In the convective limit, particle trajectories are defined by $\psi = \mathrm{const}$. This constraint implies that $\psi(r, \theta) = \psi(R, \pi/2N) = R^{-N}$, or $r^N = R^N\sin(N\theta)$, where R is the maximum distance from the origin on the streamline. The angular velocity on such a streamline is

$$r\frac{d\theta}{dt} = u_\theta = -\frac{\partial \psi}{\partial r} \sim Nr^{N-1}\sin(N\theta), \quad (33a)$$

which can be reexpressed as

$$\frac{d\theta}{dt} \sim R^{-N-2}\sin^{-2/N}(N\theta). \quad (33b)$$

The transit time on such a trajectory is the time required for θ to vary between 0 and π/N. If we neglect the small time interval spent in the near-field region at the end points and use the above approximation for the angular velocity everywhere, the transit time is approximately

$$t = \int_0^{\pi/N} \frac{d\theta}{d\theta/dt} \sim R^{N+2}. \quad (34)$$

To determine the transit time distribution, we must relate the value of R to the initial angle of emission θ_0 at the source. Suppose the source is at the origin and oriented so that the long-excursion steamlines are associated with $\theta_0 \to 0$. For $r \to \epsilon$, $\psi = R^{-N} \to \epsilon^{-N}\sin\theta_0 \to \epsilon^{-N}\theta_0$ or $\theta_0 \sim R^{-N}$. Thus the transit time probability distribution is

$$p(t) = p(\theta_0) \left| \frac{d\theta_0}{dt} \right| = \frac{1}{2\pi} \left| \frac{d\theta_0}{dR} \frac{dR}{dt} \right|$$

$$\sim R^{-2N-2} \sim t^{-(2N+2)/(N+2)}. \quad (35)$$

For example, for $N = 2$ (quadrupole), the flow field has the four-lobed structure shown in Fig. 12 and the exponent of the transit time distribution is $-\frac{3}{2}$. Another

example is the "five-spot" shown in Fig. 16, consisting of a source (injection well) surrounded by four sinks (production wells). This flow configuration is widely used in petroleum recovery. In practice, this pattern is replicated, roughly periodically, but we focus here on an isolated unit cell. The five-spot is an $N=4$ (16-pole) configuration in two dimensions [as can be verified by working out the coefficients in Eq. (32)] rather than a quadrupole in the familiar three-dimensional multipole expansion. If we take the source and each sink to have strength Q and $-Q/4$, respectively, and then integrate along trajectories, we find a transit time distribution with the expected $t^{-5/3}$ decay (Fig. 17). For a periodically repeated five-spot, there would be the additional effect of slow diffusive transport between unit cells. Analogous behavior is found for tracer motion in a Rayleigh-Bénard convection cell pattern, where the intra- and intercell motion yields two distinct time scales [15]. Here the in-

tracell motion already entails the long time scale, so the analogy is not complete.

An example that nicely illustrates crossover behavior between different multipolarities is a quadrupole in which the source is displaced slightly below the x axis (Fig. 18). This displacement implies that the flow field is actually dipolar at large distances, so that the penultimate decay of $p(t)$ should be characterized by the dipolar exponent. However, closer to the source and sinks the flow is approximately quadrupolar, and to the extent that specific parameters permit the inner quadrupole pattern to persist over some distance, one might hope to see the $t^{-3/2}$ quadrupole decay over a corresponding time interval. The transit time distribution, obtained by integrating along specific trajectories, reflects these different regimes. Streamlines that emerge from the origin near $\theta=\pi/2$ are quadrupolar, except for those very near the y axis, which are attracted toward a stagnation point. This subgroup
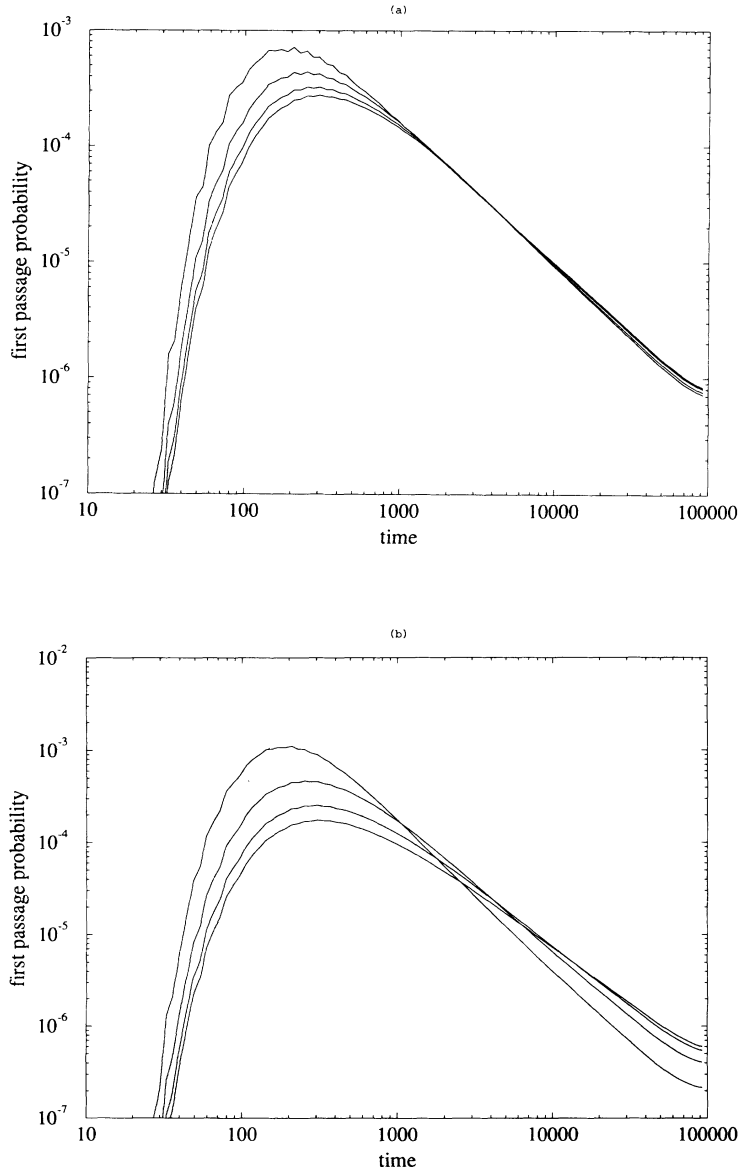

FIG. 14. Transit time probability distribution for combined quadrupolar flow and diffusion within a circle of radius $R=300$ based on probability propagation. Shown are (a) the quadrupole with point singularities at $(-a,0,+a)$ of strength $(-Q,2Q,-Q)$ and (b) the inverted quadrupole with point singularities located at $(-a,0,+a)$ of strength $(Q,-2Q,Q)$. In both cases, $a=20$. Shown are the distributions for the representative set of Péclet numbers Pe $= 1.6, 0.8, 0.4$, and 0.2 (tallest to shortest peaks, respectively).

of trajectories give rise to $p(t) \sim t^{-3/2}$ over some time range, followed by an exponential cutoff (Fig. 19). For streamlines emerging near $3\pi/2$, those which are not too close to the y axis are also quadrupolar, leading to a $t^{-3/2}$ contribution to $p(t)$, whereas streamlines closer to the y axis are carried farther out into the dipolar flow region and there is a crossover to the slower $t^{-4/3}$ decay for $p(t)$ at longer times.

D. Flows in a wedge geometry

A configuration of theoretical and potential practical interest occurs for a source inside a *wedge*, as might result when a well lies between two intersecting underground streams, which act as adsorbing boundaries for tracer particles. Suppose a unit source is placed at $(1,0)$, the sides of the wedge $\theta = \pm\alpha/2$ are equipotentials where $\phi = 0$, and the wedge has a finite size, closed at large distances by the arc $r = R$ (the streamlines for the case $\alpha = \pi/3$ are plotted in Fig. 20). The potential flow problem is easily solved by transforming the region into the right half plane, using the conformal mapping $w = z^{\pi/\alpha}$ to recast the system as simple dipole flow whose potential is given in Eq. (16) (except for a trivial interchange between the location of the source and the sink). Transforming this solution back to the original geometry, the velocity potential is

$$\Psi = \ln \frac{(z^{\pi/\alpha} - 1)(z^{\pi/\alpha} - R^{2\pi/\alpha})}{(z^{\pi/\alpha} + 1)(z^{\pi/\alpha} + R^{2\pi/\alpha})} \ . \tag{36}$$

Consider a passive tracer that is released at the source and collected in the "streams" at the wedge sides. The trajectories that control the tail of $p(t)$ are those directed toward the arc at $r = R$, at which point the flow becomes tangential, and the tracer is then collected. These paths are quite similar to the lobelike trajectories that occur in multipole flows. The primary difference between the two cases is that for the wedge the asymptotic behavior of Ψ is seen from Eq. (36) to be $\Psi \sim z^{-\pi/\alpha}$, instead of z^{-N} as in the case of a 2^N pole. The argument to determine the exponent for $p(t)$ can be essentially copied from the mul-
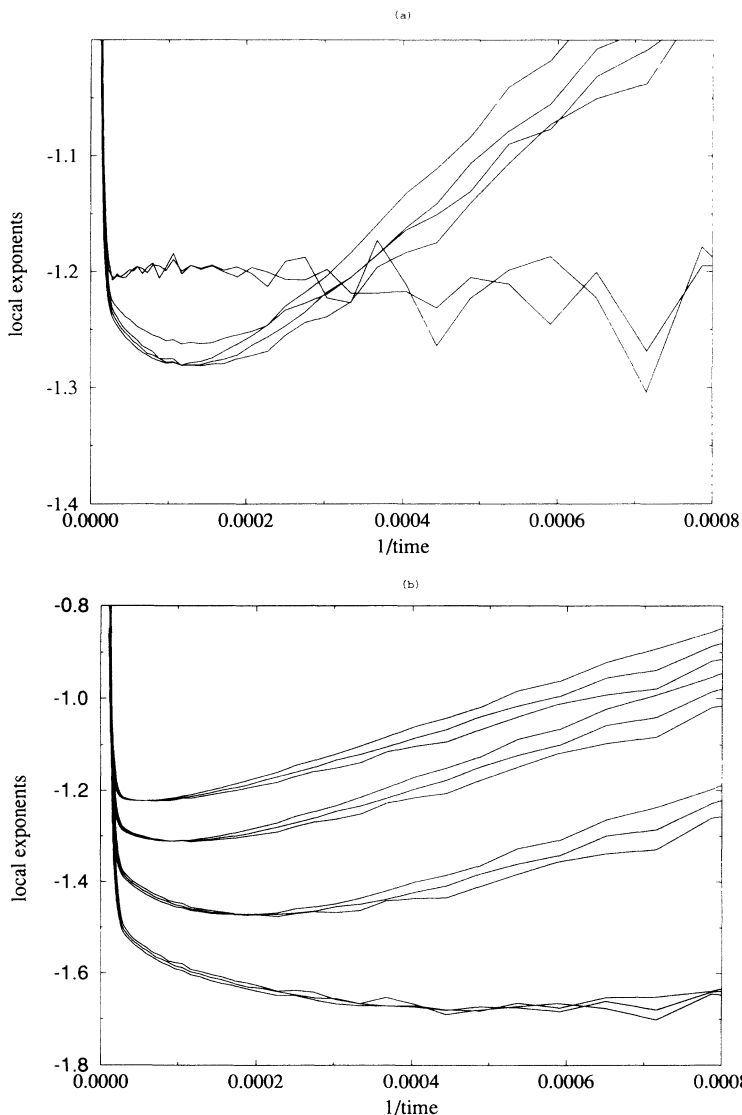

FIG. 15. The local exponent of the transit time distribution, based on slopes of successive second-neighbor, fourth-neighbor, and sixth-neighbor points in Fig. 14, plotted vs $1/t$. (a) For the quadrupole, data sets for Pe = 1.6 (jagged at early times) and Pe = 0.2 are shown. In the power-law regime, both data sets indicate an exponent of approximately -1.2. (b) For the inverted quadrupole, the lower to upper curves correspond to decreasing values of Pe. For the largest Péclet number simulated, the local exponent may be compatible with an asymptotic value of $-\frac{3}{2}$. For smaller Péclet numbers, the local exponents appear to extrapolate to an asymptotic value which depends on the Péclet number.
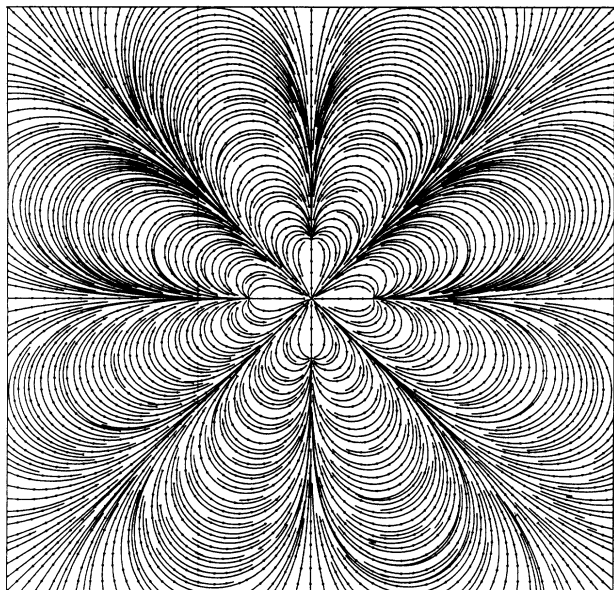
FIG. 16. Streamlines for the "five-spot" octupole flow.

FIG. 18. Streamlines for "perturbed" quadrupolar flow.

tipole case upon making the substitution $N \to \pi/\alpha$. Thus, for wedge flows,

$$p(t) \sim t^{-n} \quad \text{with} \quad n = \frac{2\pi + 2\alpha}{\pi + 2\alpha} \quad (\text{Pe} \to \infty) \ . \tag{37a}$$

A direct numerical integration of the trajectories for several values of α confirms this exponent value. At very long times, however, the distribution is cut off exponentially due to the stagnation point at the boundary $r = R$. In the opposite limit of pure diffusion in an infinite wedge, it is well known [16] that the transit time distribution decays as

$$p(t) \sim t^{-1-\pi/2\alpha} \quad (\text{Pe} \to 0) \ . \tag{37b}$$

Although a power-law decay is found for both pure diffusion and pure convection, the exponent is nonuniversal and depends on both the wedge geometry and Pe. In

particular, the mean transit time always diverges in the convective limit for $R \to \infty$, as the general theorem cited in the Introduction requires. In the diffusive limit the mean transit time is finite when the wedge angle is less than $\pi/2$ and the mean time is divergent otherwise. Roughly speaking, in a sufficiently narrow wedge a tracer tends to diffuse to the walls relatively quickly, whereas a flow always advects some tracer out into the center of the wedge, where a long time is required for it to reach the sides, and narrowing the wedge simply focuses these streamlines.

E. Flows in the presence of barriers

In the field, one often has impermeable barriers to flow in an otherwise permeable region [1]. A barrier can significantly distort the streamlines of the flow and modi-

FIG. 17. Transit time probability distribution for the five-spot flow in the convective limit.

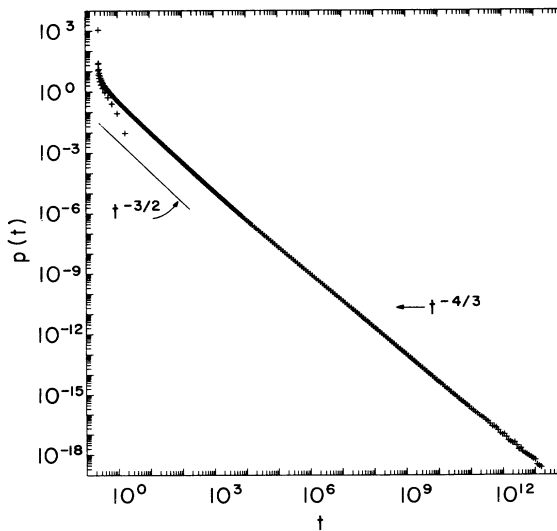FIG. 19. Convective transit time distribution corresponding to Fig. 18; note the crossover from quadrupolar $(t^{-3/2})$ to dipolar $(t^{-4/3})$ behavior.
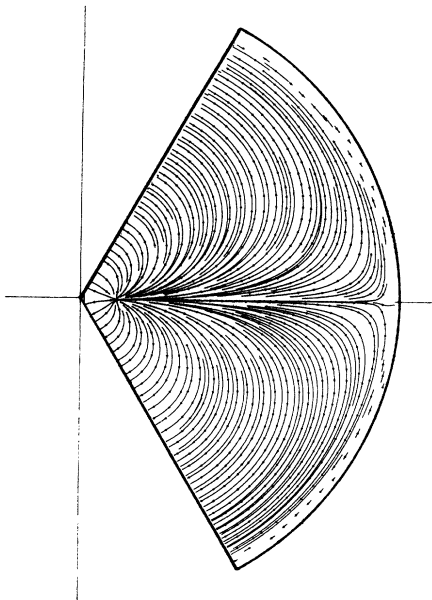
FIG. 20. Streamlines for convection within an absorbing wedge of opening angle $\pi/3$.

fy the transit time distribution. We have considered two extreme cases of barriers, which illustrate situations in which such a major distortion does or does not occur, asymptotically.

Consider first a case involving a "localized" barrier, in which a source and a sink at $x = \pm 1$, respectively, are separated by an impermeable barrier extending along the y axis from $-b$ to $+b$. The unperturbed streamlines, which run more or less directly from the source to the sink, must now detour around the barrier, and the early time portion of $p(t)$ is certainly altered. However, the power-law tail is associated with the streamlines which initially move away from the barrier and sweep around the barrier at a large transverse distance from the end, before reaching the sink. These large-distance streamlines are negligibly altered by the presence of the barrier and one expects the usual dipole behavior to ensue. The result can be seen quantitatively, and in a form easy to generalize, by considering the complex potential.

To solve the finite barrier flow problem, consider the conformal transformation $z = ib(w + 1/w)/2$, which maps the interior of the unit circle in the w plane into the full z plane, with the unit circle in w mapped into the line $-b \le \mathrm{Im}(z) \le b$. Thus the original problem in the z plane maps into one of potential flow in w with a source and a sink symmetrically located at $w_{1,2}$ and an impermeable circular boundary at $|w| = 1$. This is precisely the simple dipole flow considered in Sec. III, with complex potential

$$\Phi(w) = \ln \frac{(w - w_1)(w - \bar{w}_1)}{(w - w_2)(w - \bar{w}_2)} , \tag{38}$$

where $\bar{w}_{1,2}$ are the image positions. At large z, $w \to ib/2z \to 0$, leading to

$$\Psi \to c_1 + c_2 w = c_1 + \frac{c_3}{z} , \tag{39}$$

where the c_i are constants. Equation (39) is precisely the asymptotic form of the potential for dipole flow and

therefore the dipole decay exponent applies at long times.

To illustrate a case wherein a barrier alters the asymptotic form of $p(t)$, consider now a semi-infinite impermeable barrier extending along the full negative x axis, with a source and a sink above and below the barrier, respectively. Again, the asymptotic behavior of $p(t)$ follows from the geometry of the far streamlines, which in turn follows from the asymptotic behavior of $\Psi(s)$. In this case, the barrier is the same as a wedge whose sides are at $\theta = \pm\pi$, and in analogy to Sec. IV D we map the *exterior* of the wedge into the right half plane using the conformal transformation $w = z^{1/2}$. The barrier maps into the y axis and the source and the sink lie somewhere in the right half plane at $w_{1,2}$. The flow problem is solved again using the method of images, with a solution of the form Eq. (36), but now with images $\bar{w}_{1,2}$ in the *left* half plane. With this mapping, the $z \to \infty$ limit corresponds to $w \to \infty$, whence $\Psi \to 1/w = z^{-1/2}$. Proceeding again by analogy to the wedge arguments above, the asymptotic decay of Ψ is equivalent to a multipole of order $N = 1/2$ and from Eq. (35) we have

$$p(t) \to t^{-6/5} \quad (\mathrm{Pe} \to \infty) . \tag{40}$$

A direct numerical integration in the pure-convection limit confirms this power-law decay exponent.

Examples of crossover behavior can occur for a finite barrier when, for example, the source and the sink are very close to the center of the barrier while at the same time being very far from its edges. While the ultimate asymptotic behavior is that of a dipole, tracer particles that initially head from the source toward the middle of the barrier and then bend and wrap around it to reach the sink are the same as those encircling a *semi-infinite* barrier and would have the behavior indicated in Eq. (40). Furthermore, trajectories directed close to the center of the barrier would pass near a stagnation point and would be associated with an exponential decay in $p(t)$. Thus, for this geometry one has a power-law decay whose exponent crosses over from $\frac{6}{5}$ to $\frac{4}{3}$, in addition to the exponential branch.

It is evident from these examples that there is no general exponent that characterizes the decay of $p(t)$ for all barriers. On the other hand, it is equally evident that the asymptotic behavior of particular cases can be worked out by determining the analytic form of the velocity potential and in favorable case inferred from a sketch of the streamlines.

V. CONCLUSIONS

We have investigated the transit time properties of passive tracer particles in a variety of steady two-dimensional potential flows between sources and sinks. We have focused attention on a range of illustrative case studies. In radial flows, the interplay between convection and centrifugal diffusion leads to a nonuniversal power-law decay of the transit time probability distribution $p(t)$. For pure 2^N-polar convection, $p(t)$ is found to decay as $t^{-(2N+2)/(N+2)}$. This was verified by a complete solution of the dipolar problem and by consideration of the "critical" streamlines for the arbitrary case. There are also strong orientation-dependent features associated with

those subpopulations of tracer which are attracted to stagnation points in the flow field. Furthermore, one has regimes of exponential decay which may be associated with stagnation points in the interior of the flow domain as well as its boundary. When diffusion is also present, some of the generic features of the transit time probability become more system specific. For spatially extended sinks, we have shown that the spatial distribution of the collected tracer is independent of the overall magnitude of the flow field.

The practical consequences of this paper are that for planar multipole flows, the transit time distribution and, in particular, its power-law decays, cutoffs, and shoulders reflect the geometry of sources, sinks, and boundaries of the porous medium in the manner summarized in Sec. III B. A given power of t indicates a particular multipole moment of the source-sink distribution, a shoulder indicates rebounding from the boundary of the permeable region, and an exponential decay indicates stagnation points in the flow. We hope that such obvious features of the tracer distribution may permit one to characterize a subsurface porous medium by relatively simple and inexpensive surface measurements. Commonly in porous media studies one is interested in the effective dispersion coefficients of the porous medium. We have argued that these are entirely irrelevant for the generic features of the transit time distribution, but instead manifest themselves in various numerical coefficients in $p(t)$. We have not studied this (weak) dependence of the transit time distribution on effective dispersivity because other flow configurations exist (e.g., core flow) that are more sensitive to these quantities.

There are several interesting directions that might be suitable for additional investigation. First, it is most important to extend our predictions for multipole and other flow configurations to three dimensions. Although the full power of complex analysis methods are no longer applicable, the two-dimensional systems considered were sufficiently simple that alternative methods of study may be available in three dimensions. Although we have argued that a planar porous medium is a viable starting point, realistic media have a fully three-dimensional structure. A change in dimension will certainly change the values of power-law exponents and could well alter some of our qualitative results as well. An equally significant additional consideration is the presence of spatial heterogeneities. One may distinguish two cases depending on whether the disorder is strong enough to qualitatively change the far-field behavior of the streamlines. If the number and the gross shape of the lobes in ψ are unchanged, then it is evident from the arguments above for composite sinks that exponents will not change. In the other extreme, as in the semi-infinite barrier example, a large-enough heterogeneity may alter the whole streamline pattern and change the decay law. In addition to providing a more realistic component to the modeling, strong disorder may provide new qualitative features in transit time properties.

ACKNOWLEDGMENTS

APPENDIX A: GREEN'S FUNCTION FOR THE CDE IN AN ANNULUS

We solve for the Green's function in Laplace space for the radial convection-diffusion equation

$$c'' - \frac{Pe-1}{x}c' - c = -\frac{\delta(x-x_0)}{2\pi x_0} , \qquad (A1)$$

with $c(a)=0$ and $-c'+(Pe/x)c|_{r=R}=0$. Here the derivative is with respect to dimensionless coordinates, which have been rescaled by the factor $\sqrt{s/D}$. Since the discussion that follows is consistently for Laplace transformed quantities, the tilde and the Laplace variable s are generally not written. The above differential equation has the standard form of Bessel's differential equation. The Green's function is therefore a superposition of modified Bessel functions of both the first and second kinds, $I_\nu(x)$ and $K_\nu(x)$, respectively, because the range of x is finite. Since the interior Green's function (defined for $a \leq x < x_0$) equals zero at $r=a$, it can immediately be written in a symmetric form that manifestly vanishes at the inner circle. Thus

$$c_<(x) = Ax^\nu[I_\nu(x)K_\nu(a)-K_\nu(x)I_\nu(a)] ,$$
$$c_>(x) = -x^\nu[BI_\nu(x)+CK_\nu(x)] , \qquad (A2)$$

with $\nu = Pe/2$. We now apply the remaining boundary condition, together with appropriately matching the interior and exterior Green's function at $x=x_0$, to determine the unknown coefficients.

At $x=R$, the vanishing of the flux implies that

$$c_>'|_{x=R} = \frac{Pe\, c_>(R)}{R} . \qquad (A3)$$

The first derivative $c_>'$ is found from the recursion relations

$$I_\nu' = -\frac{\nu}{x}I_\nu + I_{\nu-1} , \quad K_\nu' = -\frac{\nu}{x}K_\nu - K_{\nu-1} . \qquad (A4)$$

Notice that in differentiating $c_>'$, the factor that stems from differentiating the factor x^ν is conveniently cancelled by the term in Eq. (A4) that involves the Bessel function of order ν. Thus the derivative reduces to

$$c_>'(x) = x^\nu[BI_{\nu-1}(x)-CK_{\nu-1}(x)] \qquad (A5)$$

and Eq. (A3) now gives

$$R^\nu[BI_{\nu-1}(R)-cK_{\nu-1}(R)] = \frac{Pe}{R}R^\nu[BI_\nu(R)+CK_\nu(R)] . \qquad (A6)$$

We therefore obtain

$$C = B\frac{I_{\nu-1}(R)-PeI_\nu(R)/R}{K_{\nu-1}(R)-PeK_\nu(R)/R} = B\frac{I_{\nu+1}(R)}{K_{\nu+1}(R)} . \qquad (A7)$$

Using this in Eq. (A2) yields

$$c_>(x) = B \frac{x^\nu}{K_{\nu+1}(R)} [I_\nu(x)K_{\nu+1}(R) + K_\nu(x)I_{\nu+1}(R)] .$$

(A8)

To fix A and B, we first impose continuity of the Green's function at $x = x_0$. After simple manipulations, the two components of the Green's function can be written in the symmetric forms

$$c_<(x) = Ax^\nu[I_\nu(x)K_\nu(a) - K_\nu(x)I_\nu(a)]$$
$$\times [I_\nu(x_0)K_{\nu+1}(R) + K_\nu(x_0)I_{\nu+1}(R)] ,$$
$$c_>(x) = Ax^\nu[I_\nu(x_0)K_\nu(a) - K_\nu(x_0)I_\nu(a)]$$
$$\times [I_\nu(x)K_{\nu+1}(R) + K_\nu(x)I_{\nu+1}(R)] .$$

(A9)

By integrating (A1) across the discontinuity at x_0, the last condition in the Green's function is

$$c_>' - c_<' = -\frac{1}{2\pi x_0} ,$$

(A10)

where the derivatives are evaluated at x infinitesimally greater than and infinitesimally less than x_0, respectively. In computing c', note that by (A4), there are contributions that are proportional to c itself, but these can be ignored because of the continuity of the Green's function at $x = x_0$. Thus we only need to retain the term in the derivative where the order of the Bessel function is reduced by one. The relevant term for $c_>' \big|_{x=x_0^+}$ is

$$Ax_0^\nu[I_\nu(x_0)K_\nu(a) - K_\nu(x_0)I_\nu(a)]$$
$$\times [I_{\nu-1}(x_0)K_{\nu+1}(R) - K_{\nu-1}(x_0)I_{\nu+1}(R)] ,$$

while the relevant term for $c_<' \big|_{x=x_0^-}$ is

$$Ax_0^\nu[I_{\nu-1}(x_0)K_\nu(a) - K_{\nu-1}(x_0)I_\nu(a)]$$
$$\times [I_\nu(x_0)K_{\nu+1}(R) - K_\nu(x_0)I_{\nu+1}(R)] .$$

For these relevant terms, we now impose the condition Eq. (A10). After several simple but cumbersome steps, and using the Wronskian relation

$$I_\nu(x_0)K_{\nu-1}(x_0) + K_\nu(x_0)I_{\nu-1}(x_0) = \frac{1}{x_0} ,$$

(A11)

one finds

$$A = \frac{1}{2\pi x_0^\nu} \left[\frac{1}{I_\nu(a)k_{\nu+1}(R) + K_\nu(a)K_{\nu+1}(R)} \right] .$$

(A12)

Finally, the interior Green's function is given by

$$c_<(x) = \frac{1}{2\pi} \left[\frac{x}{x_0} \right]^\nu [I_\nu(x)K_\nu(a) - K_\nu(x)I_\nu(a)]$$
$$\times \left[\frac{I_\nu(x_0)K_{\nu+1}(R) + K_\nu(x_0)I_{\nu+1}(R)}{I_\nu(a)K_{\nu+1}(R) + K_\nu(a)I_{\nu+1}(R)} \right] .$$

(A13)

From this interior Green's function, the flux to the absorbing circle is given by $j\big|_{r=a} = 2\pi a c_<' \big|_{r=a}$. (We can ignore the convective contribution to the flux since the

concentration vanishes at the small circle.) Because the initial probability is normalized to unity and all particles that impinge on the circle $r = a$ are absorbed, the flux into the small circle coincides with the Laplace transform of the first passage or transit time probability $\bar{p}(s)$. Performing the derivative and again using the Wronskian relation Eq. (A11), we thereby find

$$\bar{p}(s) = \left[\frac{a}{x_0} \right]^\nu \frac{I_\nu(x_0)K_{\nu+1}(R) + K_\nu(x_0)I_{\nu+1}(R)}{I_\nu(a)K_{\nu+1}(R) + K_\nu(a)I_{\nu+1}(R)} .$$

(A14)

For the complementary situation of reflection at $r = a$ and absorption at $r = R$, the transit time probability to the outer circle can be obtained from Eq. (A14) by the interchange $a \leftrightarrow R$.

APPENDIX B: PURE CONVECTION IN AN INFINITE 2D DIPOLE FLOW

We wish to find the trajectories of particles advected in the dipole velocity field

$$\mathbf{u} = \nabla\phi , \quad \phi = \text{Re}(\Psi) , \quad \Phi = \ln\frac{z+1}{z-1} ,$$

which is equivalent to the equations

$$\dot{x} = \frac{\partial\psi}{\partial y} , \quad \dot{y} = -\frac{\partial\psi}{\partial x}$$

with $\psi = \text{Im}\Psi = \tan^{-1}\frac{2y}{1-x^2-y^2} .$ (B1)

The latter are the equations of a conservative Hamiltonian system where x is a coordinate, y is a momentum, and ψ is the energy. Our method of solution is to find a canonical transformation to a coordinate-momentum pair (p,q) whose transformed Hamiltonian $K(p,q)$ is simple. In the notation of Goldstein [17], we seek a generating function $F_2(x,p)$ such that

$$y = \frac{\partial F_2}{\partial x} , \quad q = \frac{\partial F_2}{\partial p} , \quad K = H$$

(B2)

with the special requirement $K = p$, so that the equations of motion simplify to $\dot{p} = 0$ and $\dot{q} = 1$.

We first illustrate the method with the simple case of pure radial flow, where $\Psi = \ln z$ and $\psi = \tan^{-1}(y/x)$. The condition $\psi = K = p$ implies $y = x \tan p = \partial F_2(x,p)/\partial x$, so that $F_2 = \frac{1}{2}x^2\tan p + f(p)$ and $q = \frac{1}{2}x^2\sec^2 p + f'(p)$. Now with $K = p$, $\dot{p} = 0$. Therefore p and hence y/x are constants and the motion is along a ray from the origin. Furthermore, $\dot{q} = 1$, leading to $t = q = \frac{1}{2}(x^2+y^2) + f'(p)$, or $r^2 = 2(t - t_0)$, the obvious solution to $\dot{r} = 1/r$.

Returning to the dipole case, we again wish to have $K = p$ so that

$$\tan p = \frac{2y}{(1-x^2-y^2)}$$

or $y = -\cot p \pm \sqrt{1 - x^2 + \cot^2 p}$

(B3)

is the equation satisfied by the particle trajectories. At $t = 0$ we have $x = -1 + \epsilon\cos\theta$, $y = \epsilon\sin\theta$, $\epsilon \ll 1$, corresponding to the release of the tracer from a small circle about $x = -1$ at angle θ, so that $p = \theta + O(\epsilon)$. In order

for y to remain finite as $p \to 0$ the plus sign in the second equation is required. We obtain the generating function from Eq. (B2) as

$$F_2(x,p) = -x \cot p$$
$$+ \tfrac{1}{2}[x \sqrt{\csc^2 p - x_2}$$
$$+ \csc^2 p \, \sin^{-1} x \, \sin p] + f(p) \qquad \text{(B4)}$$

and the trajectories are

$$q = t = \frac{\partial F_2}{\partial p}$$
$$= \csc^2(p)[x - \cot p \, \sin^{-1}(x \sin p)] + f'(p) , \qquad \text{(B5)}$$

where the constant $f'(p)$ is fixed by the initial conditions on x and θ. As a check on these manipulations, the limiting behavior for $p, \theta \to 0$ is $t \to x/2 - x^3/6 + O(p^2) + f'(0)$, which can be verified directly. In general, the trajectories are symmetric about the y axis, so the transit time is

$$t^* = 2t(x=0) = 2\csc^2(p)[\cot p \, \sin^{-1} x_0 \sin p - x_0]$$
$$\underset{\epsilon \to 0}{\longrightarrow} 2\csc^2(\theta)[1 - \theta \cot \theta] . \qquad \text{(B6)}$$

For more complicated flows this method unfortunately becomes too cumbersome to be useful. For example, for a dipole inside a circle, the condition $\psi = p$ is a quartic equation for y and it is awkward to find F_2.

APPENDIX C:
THE PROBABILITY PROPAGATION ALGORITHM

We are concerned with the probability distribution $c(\mathbf{r}, t)$ that random walkers released from the source at time 0 are at point $\mathbf{r}$ at time t. Suppose that at time t one has probability $c_{i,j}(t) \equiv c_0$ for a random walker to be at site i, j on a two-dimensional lattice of spacing l. In time Δt, this probability is first translated through a distance $\Delta \mathbf{r} = \mathbf{u}(\mathbf{r})\Delta t$ to a position (x,y), which is not in general a lattice site, and then redistributed to the nearest-neighbor sites of the new position. The redistribution rule is chosen to ensure that the average displacement is $\Delta \mathbf{r}$ and that the fluctuation in displacement is constant. In effect, the probability propagation method is a finite difference calculation with a particular (physical) form of interpolation.

Referring to Fig. 21, if we choose the origin of coordinates $(0,0)$ at the lattice site closest to (x,y), and for the moment return to physical units, then we require that

$$l[c_{1,0} - c_{-1,0}] = x , \quad l[c_{0,1} - c_{0,-1}] = y , \qquad \text{(C1)}$$

so that the mean location of the probability is (x,y) and

$$(l-x)^2 c_{1,0} + x^2[c_{0,1} + c_{0,0} + c_{0,-1}]$$
$$+ (l+x)^2 c_{-1,0} = 2D_x \Delta t ,$$
$$(l-y)^2 c_{0,1} + y^2[c_{1,0} + c_{0,0} + c_{-1,0}] \qquad \text{(C2)}$$
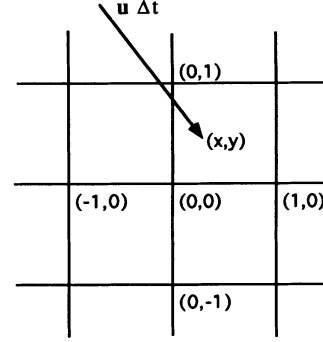$$+ (l+y)^2 c_{0,-1} = 2D_y \Delta t ,$$

FIG. 21. Illustration of diffusive redistribution in the probability propagation algorithm.

so that the mean square displacements correspond to diffusion. We have allowed for anisotropic dispersion coefficients $D_{x,y}$ for generality. Finally, we have

$$c_{0,0} + c_{1,0} + c_{-1,0} + c_{0,1} + c_{0,-1} = c_0 \qquad \text{(C3)}$$

to conserve probability. Notice that with five constraints, five-site spreading is the simplest possibility; if more spreading were desired, higher-moment constraints should be considered as well. The solution of these equations is

$$c_{0,0} = 1 - [x^2 + y^2 + 2(D_x + D_y)\Delta t]/l^2 ,$$
$$c_{1,0} = [2D_x \Delta t + x(l+x)]/2l^2 ,$$
$$c_{-1,0} = [2D_x \Delta t - x(l-x)]/2l^2 , \qquad \text{(C4)}$$
$$c_{0,1} = [2D_y \Delta t + y(l+y)]/2l^2 ,$$
$$c_{-1,0} = [2D_y \Delta t - y(l-y)]/2l^2 ,$$

which should be applicable in the range $|x|, |y| \le l/2$.

A surprising constraint is implied by these equations. Taking $D_x = D_y = D$ for simplicity and letting $d = 2D\Delta t /l^2$, if $x = y = l/2$, then $c_{0,0} = \tfrac{1}{2} - 2d$, while if $x = l/2$ and $y = 0$, then $c_{-1,0} = \tfrac{1}{2}(d - \tfrac{1}{4})$. Since $c_{i,j}$ must be positive, $d = \tfrac{1}{4}$ is the only possibility, and recalling the definition of d, this constrains the space and time step lengths. A further constraint is that the convection displacement $|\mathbf{u}\Delta t|$ should not exceed $2l$; the maximum velocity occurs at one site from the source or the sink, where $u = Q/2\pi l$, which leads to $\Delta t < 4\pi l^2/Q$. Combining the two constraints, one finds the bound Pe < 16! The relatively strong bound could be avoided at the expense of additional complication by using a variable-size lattice or spreading to more than five sites, but we have not explored these possibilities. Another peculiarity of this algorithm is that it does not always interpolate smoothly as a function of x and y. For example, if the convection point (x,y) varies from $(n + \tfrac{1}{2} - \epsilon, 0)$ to $(n + \tfrac{1}{2} + \epsilon, 0)$, it is easy to check that $c_{n,j}$ and $c_{n+1,j}$ for $j = 0, \pm 1$ jump by finite amounts. Despite these difficulties, the probability propagation method has one distinct advantage— extreme simplicity and ease of programming.

APPENDIX D: THE REBOUND SHOULDER FOR DIFFUSION IN FINITE DOMAINS

If the tracer is released near a sink in the presence of a distant reflecting boundary, then at early times, the distant boundary plays no role and the transit time probability $p(t)$ decays as $t^{-3/2}$ in one dimension. Conversely, in the long-time limit, $p(t)$ decays exponentially in time. While the analysis of these two limiting behaviors is straightforward, there are subtle implications which arise from the "rebound" of the tracer from the reflecting boundary that are worth emphasizing. Thus consider

$$\frac{\partial c}{\partial t} = \frac{\partial^2 c}{\partial x^2} \quad \text{with} \quad c(0,t) = \frac{\partial c}{\partial x}(1,t) = 0 \qquad \text{(D1)}$$

and with the initial condition $c(x,0) = \delta(x - a)$ and $0 < a \ll 1$. It is straightforward to solve for the Laplace transform $\bar{c}(x,s)$, from which the Laplace transform of the flux or the transit time probability to the absorber is

$$\bar{p}(s) = \frac{\cosh[(1-a)\sqrt{s}\,]}{\cosh\sqrt{s}} . \qquad \text{(D2)}$$

A direct numerical inversion of this expression leads to a transit time probability distribution that exhibits a shoulder, shown in Fig. 22(a). We attribute this enhancement to the contribution of probability density which "rebounds" for the reflecting boundary. This interpretation is based on first examining the limiting behavior of $\bar{p}(s)$. For relatively short times, where the tracer has reached the near boundary at $x = 0$ but not the far boundary at $x = 1$, $a^2 \ll t \ll 1$, the relevant range of the Laplace variable is $s \gg 1$, but $a^2 s \ll 1$. For this range of s a Taylor expansion gives $\bar{p}(s) \sim 1 - a\sqrt{s} - a^2 s + \cdots$, which leads to

$$p(t) \sim t^{-3/2} , \quad a^2 \ll t \ll 1 . \qquad \text{(D3)}$$

Precisely this power-law decay is seen in Fig. 22. However, the ultimate asymptotic behavior is controlled by the rightmost singularities of $\bar{p}(s)$ in the complex-s plane, which, in this case, are the poles at $\sqrt{s} = \pm i\pi/2$). This singularity structure leads to an asymptotic exponential decay

$$p(t) \sim e^{-\pi^2 t/4} , \quad t \to \infty . \qquad \text{(D4)}$$

Thus the short-time power-law behavior is ultimately cut off by an exponential decay whose time constant is of the order of the diffusion time to the boundary. At the crossover between these two regimes, there is a relative enhancement in the first-passage probability compared to a simple crossover between the two asymptotic behaviors. In Fig. 22(b) we plot the quantity $p(t)t^{3/2}$ vs time to em-
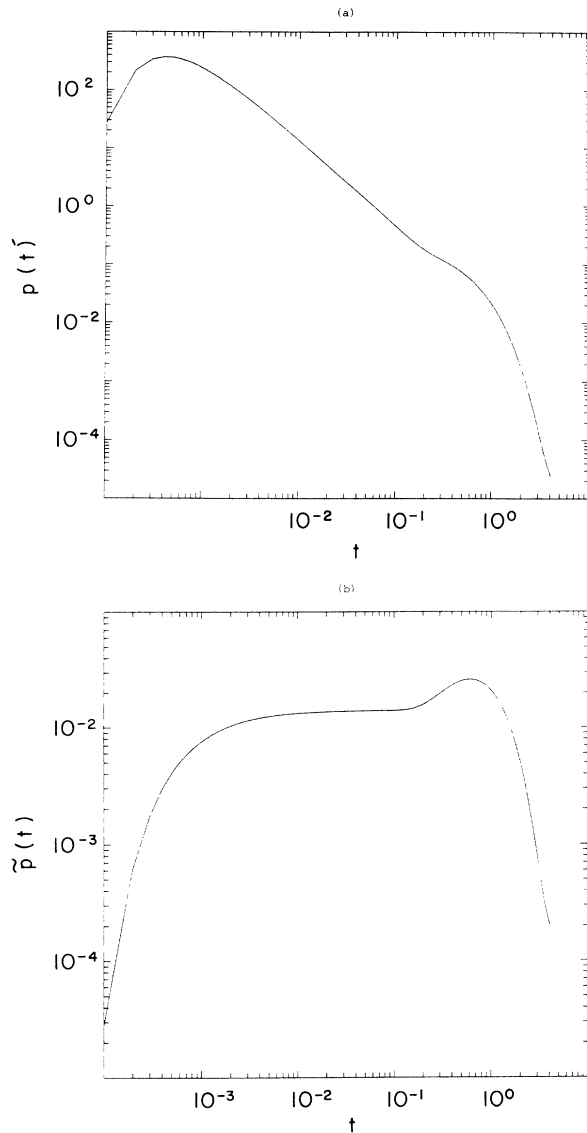

(a)

(b)

FIG. 22. Transit time probability distribution for the diffusive rebound example in one dimension: (a) $p(t)$ vs t and (b) $\bar{p}(t) = t^{3/2}p(t)$ vs t. This is a clear enhancement of the distribution relative to a pure power-law decay before exponential decay sets in.

phasize the power-law region as well as the strength of the shoulder. The location of the shoulder at the diffusion time to the boundary indicates that this enhancement stems from particles that reflect from the boundary before being collected at the sink.

[1] J. Bear, *Dynamics of Fluids in Porous Media* (Elsevier, Amsterdam, 1971).

[2] A. E. Scheidegger, *The Physics of Flow in Porous Media*, 3rd ed. (University of Toronto Press, Toronto, 1974).

[3] F. A. L. Dullien, *Porous Media: Structure and Fluid Transport*, 2nd ed. (Academic, London, 1991).

[4] M. Sahimi, Rev. Mod. Phys. **65**, 1393 (1993).

[5] *Disorder and Mixing*, edited by E. Guyon, J.-P. Nadal, and Y. Pomeau (Kluwer, Dordrecht, 1988).

[6] *Ground Water Quality*, edited by C. H. Ward, W. Giger, and P. L. McCarty (Wiley, New York, 1985).

[7] J.-C. Bacri, C. Leygnac, and D. Salin, J. Phys. (Paris) Lett. **45**, L767 (1984).

[8] E. B. Naumann and B. A. Buffham, *Mixing in Continuous*

Flow Systems (Wiley, New York, 1983).

[9] J. Koplik, S. Redner, and D. Wilkinson, Phys. Rev. A **37**, 2619 (1987).

[10] J. J. Fried and M. Combarnous, Adv. Hydrosci. **7**, 169 (1971).

[11] See, e.g., G. H. Weiss and R. J. Rubin, Adv. Chem. Phys. **52**, 363 (1983), and references cited therein.

[12] C. W. Gardiner, *Handbook of Stochastic Methods,* 2nd ed. (Springer, New York, 1985).

[13] P. Kurowski, I. Ippolito, J. P. Hulin, J. Koplik, and E. J. Hinch, Phys. Fluids **6**, 108 (1994).

[14] L. Mittag and M. J. Stephen (unpublished).

[15] A. Pumir and B. Shraiman, in *Disorder and Mixing* (Ref. [5]), p. 143.

[16] See, e.g., M. Bramson and D. Griffeath, in *Random Walks, Brownian Motion, and Interacting Particle Systems: A Festschrift in Honor of Frank Spitzer,* edited by R. Durrett and H. Kesten (Birkhauser, Boston, 1991), and references therein; D. Considine and S. Redner, J. Phys. A **22**, 1621 (1989).

[17] H. Goldstein, *Classical Mechanics,* 2nd ed. (Addison-Wesley, Reading, MA, 1980).
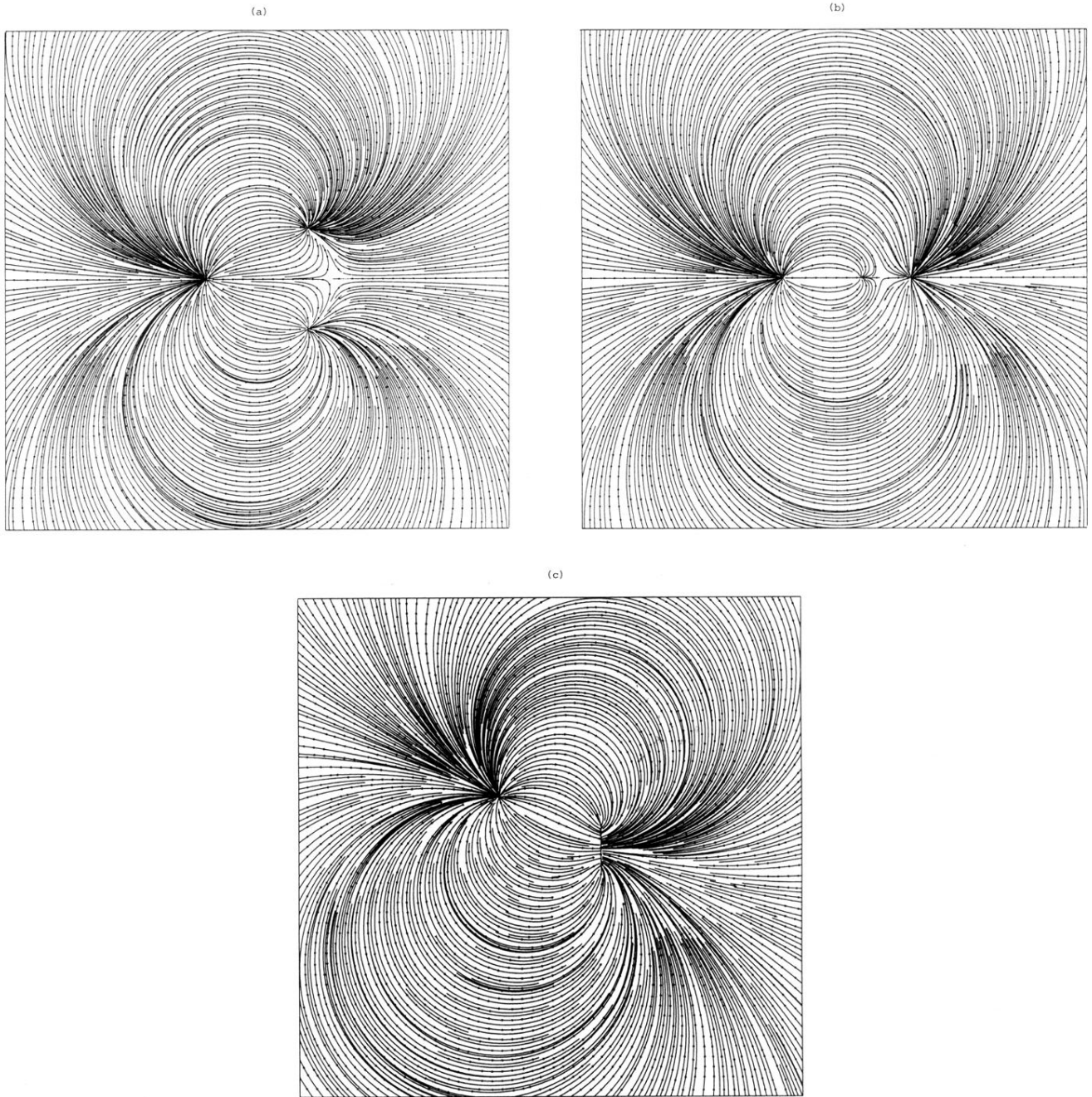
FIG. 10. Streamlines for modified dipole flow configurations: (a) a source and two sinks, each symmetrically displaced in the y direction; (b) a source and two sinks, both on the x axis; and (c) a source and a finite line sink.
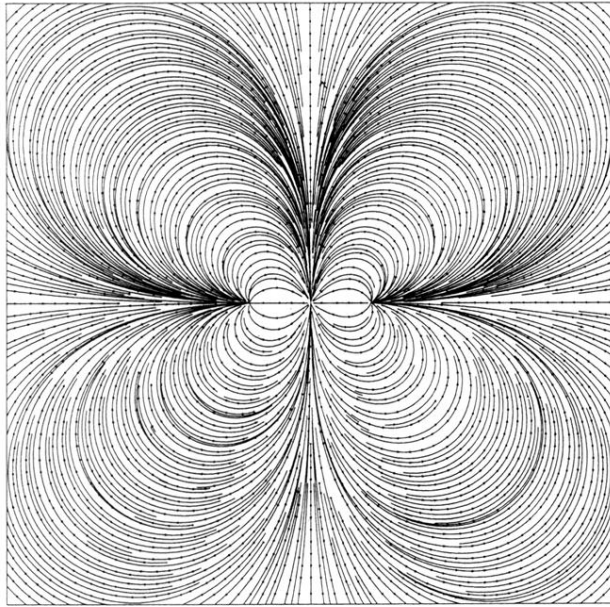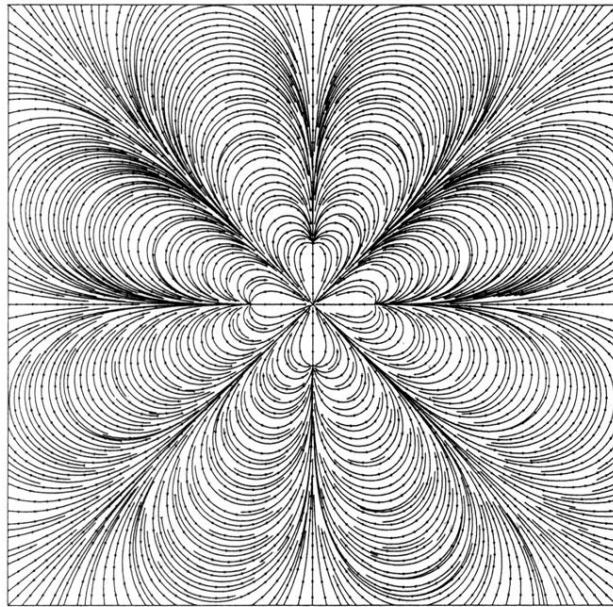
FIG. 12. Streamlines for quadrupolar flow.

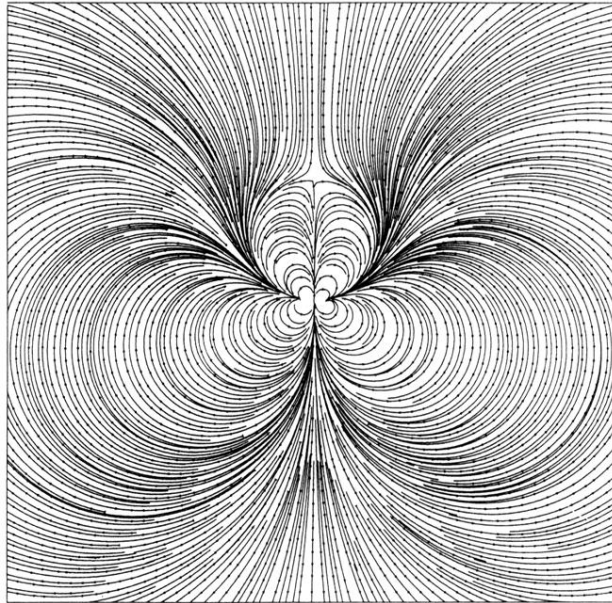FIG. 16. Streamlines for the "five-spot" octupole flow.

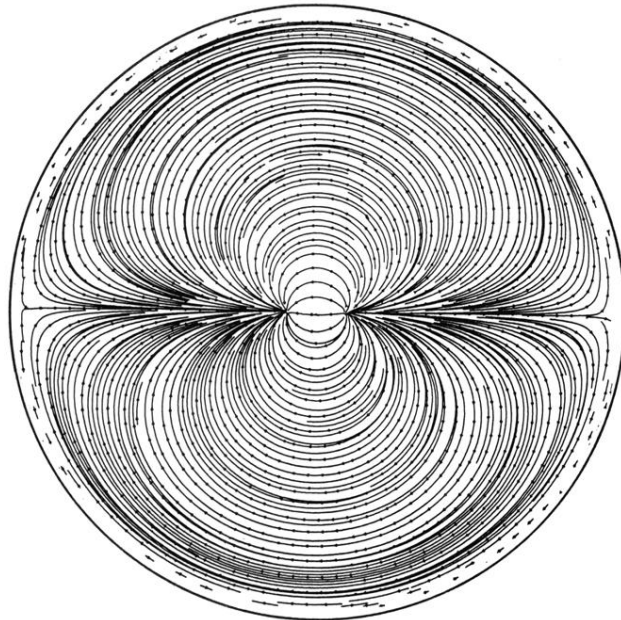FIG. 18. Streamlines for "perturbed" quadrupolar flow.

FIG. 2. Streamlines for two-dimensional dipolar flow due to a source at $x = -a$ and an equal strength sink at $x = +a$. The dipole is symmetrically placed inside a circle of radius R. Due to this geometrical constraint, the fluid flow is purely tangential along the circular boundary. Note the existence of the stagnation points at $x = \pm R$.
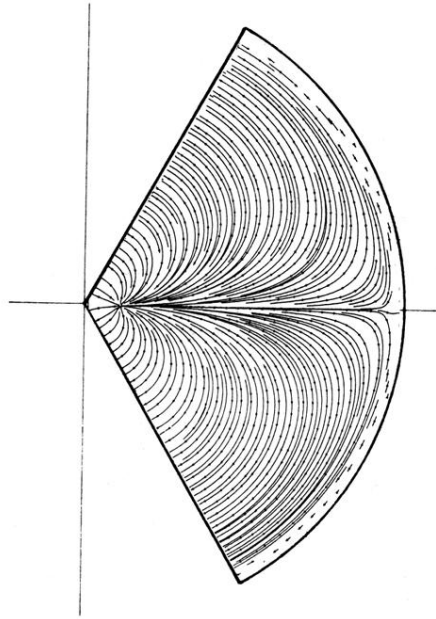
FIG. 20. Streamlines for convection within an absorbing wedge of opening angle $\pi/3$.